Sedimentary cycling and benthic fluxes of manganese, cobalt, nickel, copper, zinc and cadmium in the Peruvian oxygen minimum zone

Anna Plass[1,*], Andrew W. Dale[1], Florian Scholz[1,*]

[1]GEOMAR Helmholtz Centre for Ocean Research Kiel, Wischhofstraße 1-3, 24148 Kiel, Germany

*Corresponding authors: Anna Plass (aplass@geomar.de), Florian Scholz (fscholz@geomar.de)

Abstract

Marine sediments are an important source and sink of bio-essential trace metals to the ocean. However, the different mechanisms leading to trace metal release or burial are not fully understood and the associated fluxes are not well quantified. Here, we present sediment, pore water, sequential extraction and benthic flux data of Mn, Co, Ni, Cu, Zn and Cd along a latitudinal depth transect across the Peruvian oxygen minimum zone at 12°S. Sediments are depleted in Mn and Co compared to the lithogenic background. Diffusive Mn fluxes from the sediments into the bottom water (-26 to -550 µmol m^{-2} y^{-1}) are largely consistent with the rate of Mn loss from the solid phase (-100 to -1160 µmol m^{-2} yr^{-1}) suggesting that 50 % or more of the sedimentary Mn depletion is attributed to benthic efflux. In contrast, benthic Co fluxes (~ -3 µmol m^{-2} yr^{-1}) are lower than the rate of Co loss from the solid phase (up to -120 µmol m^{-2} yr^{-1}), implying Co dissolution in the water column. The trace metals Ni, Cu, Zn and Cd are enriched within the sediments with respect to the lithogenic background. Uptake of Ni by phytoplankton in the photic zone and delivery with organic matter to the sediment surface can account for up to 100 % of the excess Ni accumulation (87 to 180 µmol m^{-2} y^{-1}) in shelf sediments near the coast, whereas at greater water depth additional scavenging by Mn- and Fe-oxides may contribute to Ni accumulation. Up to 20 % of excess Cu (33 to 590 µmol m^{-2} y^{-1}) and generally less than 20 % of excess Zn (58 to 2170 µmol m^{-2} y^{-1}) and Cd (6 to 260 µmol m^{-2} y^{-1}) can be explained by delivery with fresh organic matter. Sequential extraction data suggest that the discrepancies between the known sources of Cd (and Cu) and their excess accumulation may be driven by the delivery of

allochthonous sulphide minerals precipitated from the water column. Additionally, Cu may be scavenged by downward sinking organic material. In contrast, precipitation of Zn sulphide chiefly takes place in the sediment. Diffusive Zn fluxes into the sediment (21 to 1990 µmol m^{-2} y^{-1}) match the excess Zn accumulation suggesting that Zn delivery is mediated by molecular diffusion from bottom waters. Considering the diverse behavioural pattern of trace metals observed in this study, we argue that declining oxygen and increasing hydrogen sulphide concentrations in a future ocean will modify trace metal fluxes at the seafloor and the trace metal stoichiometry of seawater.

1. Introduction

Trace metals (TM) are involved in many biogeochemical processes in the ocean For example, they are an essential component of enzymes that catalyse photosynthesis (Mn, Cu) as well as carbon (Co, Zn, Cd), nitrogen (Ni, Cu) and phosphorous (Zn) acquisition (Morel and Price, 2003; Morel et al., 2014; Lohan and Tagliabue, 2018). Unlike their abundance in the continental crust, TMs are often scarce in seawater, with concentrations in the range of nano- to picomoles per liter (Bruland and Lohan, 2006). Because of their limited availability, TMs can (co-)limit primary productivity in the ocean and limit the efficiency of the biological pump (Saito et al., 2008; Moore et al., 2013; Morel et al., 2014).

In paleoceanographic studies, TM concentrations in sediments have been used to infer past biogeochemical conditions in the water column and sediments (Brumsack, 2006). Certain TM enrichments (Ni, Cu) are indicative of high organic matter rain rates to the seafloor as well as sulphidic conditions within the sediments as a result of TM retention and burial as sulphide minerals (Tribovillard et al., 2006; Algeo and Liu, 2020). In contrast, sedimentary enrichments of Mn and Co may be indicative of hydrographically restricted conditions (Sweere et al., 2016) under which these elements become trapped within basin sediments.

A meaningful application of TM concentrations as paleo-redox or biogeochemical proxies requires a mechanistic understanding of their sources and sinks in the ocean, especially in low-oxygen environments. Temporal or permanent

depletion of oxygen in the water column above the seafloor can affect the extent to which TMs are removed from the water column and sequestered in the sediment because TM mobility is redox-dependent (Sundby et al., 1986; Morford and Emerson, 1999; Tribovillard et al., 2006; Scholz and Neumann, 2007; Scholz et al., 2011; Rigaud et al., 2013; Rapp et al., 2020). For example, sediments in the oxygen minimum zone (OMZ) off Peru are enriched in some TMs (Ni, Cu, Zn, Cd) whereas others are depleted (Mn, Co) compared to the lithogenic background (Böning et al., 2004; Little et al., 2015). Similar patterns have been observed in the OMZs offshore Chile and Namibia (Borchers et al., 2005; Böning et al., 2009). These enrichment or depletion patterns are reflected in TM concentrations in the water column. High Mn and Co concentrations in the water column of oxygen-deficient regions (e.g. Namibia, Peru, Mauretania, Mexico, California) were ascribed to reductive dissolution or remineralisation in anoxic waters or release from anoxic sediments (Johnson et al., 1996; Nameroff et al., 2002; Noble et al., 2012; Hawco et al., 2016; Rapp et al., 2019). Several studies have reported a quantitative removal of dissolved Cu, Zn and Cd within anoxic water columns of semi-restricted anoxic basins (e.g. Framvaren Fjord, Black Sea) and depletion in open-marine OMZs (e.g., Peru, Mauritania, North-East Pacific) (Jacobs et al., 1985; Tankéré et al., 2001; Janssen et al., 2014; Conway and John, 2015a; Janssen and Cullen, 2015; Roshan and Wu, 2015; Vance et al., 2016; Xie et al., 2019). However, the actual processes by which TMs are removed from the water column and delivered to the sediment are, in many cases, poorly constrained.

Potential TM delivery mechanisms to the sediment include incorporation into organic matter in the surface ocean by phytoplankton, scavenging by sinking organic material or Mn- and Fe-oxides, and sulphide precipitation. After deposition at the seafloor, TMs originally associated with fresh organic material or Mn- and Fe-oxides can be released and/or transferred to other solid phases such as refractory organic matter or sulphide minerals (Gendron et al., 1986; Shaw et al., 1990; Böning et al., 2004; Sheng et al., 2004; Vijayaraghavan et al., 2005; Audry et al., 2006; Rigaud et al., 2013; Little et al., 2015; Olson et al., 2017). Trace metal precipitation within sediments can also induce a downward-directed TM flux across the sediment-water interface. These different delivery mechanisms are difficult to distinguish based on water column or sediment solid phase data alone, because dissolution, transformation and fixation is likely to take place during early diagenesis. Collectively, these processes

97 determine the extent of TM accumulation in the sediment and, ultimately, the oceanic
98 dissolved TM inventory.

99 In this manuscript, we aim to identify and quantify mechanisms that lead to the
100 release or sequestration of Mn, Co, Ni, Cu, Zn and Cd in sediments in the OMZ off
101 Peru. Our analysis is based on porewater and solid phase data for surface sediments
102 along a sampling transect at 12°S (six stations) (Fig. 1). We assign individual delivery
103 pathways to each of these TMs by comparing diffusive benthic fluxes and accumulation
104 rates due to organic matter burial and TM speciation data from sequential extractions.
105 Our findings may help to reduce uncertainties that are associated with oceanic TM
106 mass balances (e.g. Homoky et al., 2016; Little et al., 2016; Archer et al., 2020) and to
107 parameterize TM fluxes in global biogeochemical models (Dale et al., 2015a; Homoky
108 et al., 2016; Tagliabue et al., 2018).

109

110

111 **2. Methods**

112

113 **2.1. Study area**

114 The upwelling region in the Eastern Tropical South Pacific off the coast of Peru
115 is characterised by one of the most intense OMZs in the ocean. The OMZ forms
116 through a combination of seasonal upwelling of nutrient-rich water, high rates of
117 primary productivity and subsequent oxygen consumption in subsurface waters.
118 Waters with near-complete oxygen depletion are generally located between 100 and
119 500 m water depth (Pennington et al., 2006; Karstensen et al., 2008; Thamdrup et al.,
120 2012). The biogeochemical conditions in the water column at our study sites are
121 spatially highly variable and, at the shallower stations, also temporally variable. During
122 phases of water stagnation on the shelf the water column can become anoxic and
123 depleted in nitrate (NO_3^-) and nitrite (NO_2^-) following intense denitrification (Sommer et
124 al., 2016). Hydrogen sulphide (H_2S) generated in the sediments by microbial sulphate
125 reduction can then be released to the water column and accumulate to micromolar
126 levels (Schunck et al., 2013; Scholz et al., 2016; Ohde, 2018). In contrast. oxygenation
127 events on the upper slope (down to 200 - 300 m) are linked to the passage of coastal

trapped waves. The passage of these poleward waves often occurs during (coastal) El Niño phases and is associated with the deepening of the nutricline and upper oxycline (Ulloa et al., 2001; Levin et al., 2002; Echevin et al., 2008; Gutiérrez et al., 2008; Ohde, 2018). A tracer release experiment that was carried out in our study area revealed that nutrients released into bottom waters at the Peruvian shelf (≤ 250 m depth) can potentially reach the surface ocean via transport and mixing processes (Freund, 2020). This observation highlights the relevance of benthic trace metal fluxes for biological processes in the surface ocean.

The sediments at our study sites on the Peruvian shelf (< 200 m) consist of fine grained diatomaceous and organic carbon-rich hemipelagic muds (Reimers and Suess, 1983; Suess et al., 1987; Froelich et al., 1988). The sediments on the slope consist of a mixture of phosphoritic sand, foraminiferal sand, and olive green mud (Muñoz et al., 2004). Sedimentation rates are highest on the inner shelf (75 m) at 0.47 cm y^{-1} and decrease on the outer shelf and slope to 0.14 to 0.05 cm y^{-1} (130 to 750 m) (Dale et al., 2020). The high productivity in surface waters leads to high particulate organic carbon (POC) rain rates, which reach 955 mg m^{-2} d^{-1} at 75 m and decrease offshore to 62 mg m^{-2} d^{-1} at 750 m (Dale et al., 2015b). The POC content in sediments ranges between 30 and 200 mg g^{-1}, with highest values found underneath anoxic bottom waters (Suits and Arthur, 2000; Böning et al., 2004; Dale et al., 2015b). Hydrogen sulphide in sediment pore waters reaches several tens to thousands of micromoles per litre (Suits and Arthur, 2000; Scholz et al., 2011; Noffke et al., 2012; Plass et al., 2020). The contents of sulphur bound to pyrite within the OMZ sediments are between 1 and 18 mg g^{-1}, and the contents of sulphur bound to organic matter are between 0.7 and 3.3 mg g^{-1}, with the highest values in the centre of the OMZ (Suits and Arthur, 2000; Scholz et al., 2014).

2.2 Sampling and analytical methods

The sampling took place between April and May 2017 during RV Meteor cruises M136 and M137 at six stations across the Peruvian shelf and slope between 75 m and 750 m water depth (Fig. 1). The station numbering was taken from Dale et al. (2015b) with the geographical coordinates listed in the supplement (Table S.1). Short sediment

cores (ca. 30 cm) were retrieved with a multiple corer and immediately transferred to the onboard cool room (4 °C). The supernatant bottom water above the sediment core was then sampled and filtered through 0.2 µm cellulose acetate filters (Sartorius). Subsequently, the sediment cores were sliced in vertical sections in a glove bag under Ar-atmosphere. The samples were then centrifuged, and the supernatant was filtered as before under Ar-atmosphere and transferred to acid cleaned low-density polyethylene (LDPE) bottles. Pore water and supernatant samples were acidified to pH < 1 with subboiled distilled HNO_3. Hydrogen sulphide concentrations were measured photometrically (U-2001 Hitachi spectrometer) on separate non acidified pore water samples using standard spectrophotometric techniques (Grasshoff et al., 1999). The centrifuged sediments were stored in the centrifuge tubes under Ar-atmosphere for TM analysis at the home laboratory. Separate uncentrifuged sediment samples were collected for determination of POC and total sulphur (TS) content as well as water content and porosity. All sediment and porewater samples that were not analysed on board were maintained at 4 °C.

To determine TM concentrations in the pore water, we generally followed the pre-concentration method described by Rapp et al. (2017) but with a half-automated device (Preplab). The acidified pore water samples (1 ml) were diluted with 2 ml of de-ionised water (MilliQ, Millipore) and irradiated with UV by light for 4 hours to destroy organic ligands that affect the recovery of Co and Cu. Before preconcentration the pH value of the sample was raised to 6.4 with an ammonium acetate buffer (1.5 M). Subsequently, the sample was loaded onto a chelating resin column where the seawater matrix was rinsed off. Then the column was rinsed with 1 ml of elution acid (1 M subboiled HNO_3) to collect the TMs. Trace metal concentrations in the pre-concentrated samples were measured by high resolution inductively coupled plasma mass spectrometry (HR-ICP-MS; Thermo Fisher Element XR). Trace metal concentrations were quantified by standard addition (Mn, Co) and isotope dilution (Ni, Cu, Zn, Cd). Accuracies for replicate measurements of reference seawater certified for TMs (NASS-7 and CASS-6) are listed in Table S.2. The pore water Cd data has been previously published along with benthic chamber data in Plass et al. (2020). These data are shown again here to explore the full range of TM behaviour on the Peruvian shelf.

Solid phase TM analyses was targeted at eight sampling depths per core (0.5 cm, 2.5 cm, 4.5 cm, 7cm, 11 cm, 16 cm, and 20 cm). Total digestions were used to determine total TM contents. Exactly 0.1 g of freeze dried and ground sediment was digested in 2 ml concentrated HF (suprapure) (40 %), 2 ml concentrated HNO_3 (suprapure) (65 %) and 3 ml concentrated $HClO_4$ (suprapure) (60 %) for 8 hours at 185 °C. The sample was then dried and re-dissolved with 1 ml concentrated HNO_3 (suprapure) and 5 ml deionized water (Milli-Q, Millipore) at 145 °C for 2 hours. The reference standard MESS-3 was treated in the same way to monitor the recovery of the digestion procedure.

A modified version of the four-step sequential extraction scheme of Huerta-Diaz and Morse (1990) was applied to determine host phases of TMs within the sediment. We opted to use unaltered wet sediment because drying can shift TMs from less mobile to more mobile phases and thus distort the results from the sequential extractions (Baeyens et al., 2003). For each extraction 0.5 g of wet sediment was used. To check the long-term reproducibility of the sequential extraction protocol, we included our in-house standard OMZ-2 (sediments from the Peruvian margin) into each extraction run (relative standard deviation ± 2 %, for Zn ± 9 %). The reference standard MESS-3 was also extracted along with the samples. All samples were constantly mixed on a shaking table during the extraction. After each extraction step the sample was centrifuged and the supernatant collected. The residual sediment was used for the subsequent extraction step. A full description of the extraction procedure follows:

Sequential extraction step 1, $HCl_{0.5M}$-fraction: The sediment was extracted in 20 ml of 0.5 M HCl (subboiled and distilled) and shaken for 1 hr. After centrifugation the supernatant was collected and stored for analysis. This extraction is operationally defined to dissolve TMs present as TM-monosulphides and TMs associated to amorphous (oxyhydr)oxides (Fe, Mn), carbonates and hydrous aluminosilicates (Kostka and Luther, 1994).

Sequential extraction step 2, HCl_{1M}-fraction: 15 ml of 1 M HCl (subboiled and distilled) were added to the residual sediment and shaken for 23 hr. After centrifugation and collection of the supernatant, the sediment was washed with 10 ml de-ionised water (MilliQ, Millipore) and centrifuged again. The supernatant was combined with the prior collected supernatant (1 M HCl) and stored for analysis. In principle, this extraction step is operationally defined to dissolve the same TM phases as step 1 plus

more crystalline phases and some silicates minerals (Huerta-Diaz and Morse, 1990; Kostka and Luther, 1994).

Sequential extraction step 3, HF-fraction: During this step, 10 ml of 10 M HF (suprapure) was added to the residual sediment and shaken for 1 hr. The sample was centrifuged and the supernatant collected. Then, 10 ml of 10 M HF was added to the sediment and shaken for 16 hr, before 2 g of boric acid was added to dissolve any precipitated fluoride minerals. The shaking was then repeated for another 8 hr before centrifuging and collection of the supernatant. Subsequently, the sediment was washed with 10 ml boiling de-ionised water, centrifuged again and the supernatant collected. All three supernatants collected during this extraction step were combined and stored for analysis. This extraction step is operationally defined to dissolve TMs associated with silicate minerals (Huerta-Diaz and Morse, 1990).

Sequential extraction step 4, HNO_3-fraction: For the last extraction step, 10 ml of concentrated HNO_3 (subboiled and distilled) was added to the remaining sample and shaken for 2 hr. Subsequently, the sample was centrifuged and the supernatant collected. The residual sediment was washed with 10 ml of concentrated HNO_3 (subboiled and distilled) and then with 10 ml of de-ionised water. After each washing step, the sample was centrifuged, the supernatant collected and combined with the prior collected supernatant and stored for TM analysis. This extraction step is operationally defined to dissolve TM associated with organic matter and pyrite (Huerta-Diaz and Morse, 1990).

Trace metals extracted in step 1, 2 and 4 are considered to be reactive and potentially mobile within the water column and surface sediment whereas TMs extracted in step 3 (silicate minerals) are considered to be of lithogenic origin and thus unreactive.

Concentrations of TMs (and also Al) in solutions from digestions and sequential extractions were measured by ICP-OES (VARIAN 720-ES). Due to its lower sedimentary content, Co concentrations were measured by ICP-MS (Agilent 7500). The recovery from replicate total digestions of the reference standard MESS-3 (n = 17, all within range) and the recovery from the sequential extraction method of our in-house standard OMZ-2 (n = 3, recovery > 90 % Mn, Co, Ni and Cd and >80 % Cu and Zn) are listed in Table S.3. Possible contamination during the extraction procedure was monitored using method blanks, which were treated in the same way as the samples.

Total sulphur and POC contents in freeze dried and ground sediment subsamples were determined by flash combustion in an Elemental Analyzer (Euro EA) after removal of inorganic carbon with 0.25 mM HCl (analytical grade). Precision and relative standard deviation of the measurement was ± 3 % for TS and ± 1 % for POC. Further sediment subsamples were freeze-dried for the determination of water content and porosity to convert the results from sequential extractions in mass units.

2.4 Flux calculations

To determine whether a TM is enriched or depleted relative to the lithogenic background (expressed as excess; TM_{xs}) we used the average TM and Al contents of each core and applied the following equation (Brumsack, 2006):

$$TM_{xs} = TM_{sample} - Al_{sample} * (TM/Al)_{crust} \quad \text{(Eq. 1)}$$

Positive and negative TM_{xs} represent sedimentary enrichment and depletion, respectively. The TM:Al ratio of andesite was used as the lithogenic background reference, in line with the overall andesitic composition of Peru margin sediment (Böning et al., 2004). We applied the same reference values for Mn, Ni, Cu, Zn, Cd and Al from Peruvian andesite as Little et al. (2015) (taken from the GEOROC data base (Sarbas and Nohl, 2009)). The reference value for Co was taken from average andesite (Taylor and McLennan, 1995) which is nearly identical to the local andesite Co:Al ratio (Aguirre, 1988). To determine the excess TM flux/accumulation in the sediment, TM_{xs} was multiplied by the mass accumulation rate (MAR) for each individual site (taken from Dale et al. (2020)):

$$TM_{xs} * MAR = TM_{xs}MAR \quad \text{(Eq. 2)}$$

To quantity TM delivered to or removed from the sediments via diffusive transport (F_D) across the sediment water interface, we applied Fick's first law of diffusion (Boudreau, 1997):

$$\mathrm{F_D} = -\Phi \mathrm{D_{sed}}(\mathrm{dC/dx}) \quad \text{(Eq. 3)}$$

In this equation, dC/dx is the concentration gradient between the uppermost pore water sample (0 – 1 cm sediment depth) and the bottom water. D_{sed} is the effective molecular

diffusion coefficient of a TM in the sediment, which was determined as follows (Plass et al., 2020):

$$D_{sed} = D_{sw}/(1 - \ln(\phi^2)) \quad \text{(Eq. 4)}$$

The molecular diffusion coefficients in seawater (D_{sw}) under standard conditions (Li and Gregory, 1974) were adjusted to in-situ temperature, pressure and salinity applying the Stokes-Einstein Equation. The denominator in Eq. 4 represents tortuosity which is derived from porosity (Φ) (Boudreau, 1997). In this study, a positive F_D represents a flux from the bottom into the pore water and vice versa. All data for diffusive flux calculations are listed in Tables S.5.

Trace metals are also delivered to the sediment via incorporation into phytoplankton and deposition of organic detritus on the seafloor. We approximated this flux by multiplying the average TM to carbon (TM:C) ratio in average phytoplankton (Moore et al., 2013) with POC rain rates and POC burial rates (data from Dale et al. (2015b)) for each site. These give the maximum and minimum TM fluxes, respectively. Regional TM:C ratios from the equatorial Pacific in bulk phytoplankton and diatoms are available for some TMs from Twining et al. (2011) and for (mostly) zooplankton from Collier and Edmond (1984). Compared to average phytoplankton, regional ratios are generally slightly lower for Mn, similar for Ni and Cu, and slightly higher for Co, Zn and Cd. Available TM data for suspended particles within the OMZ off Peru show elevated TM to phosphorus (TM:P) ratios compared to average phytoplankton (Ohnemus et al., 2017; Lee et al., 2018). In this study, we converted this local particulate TM:P to TM:C ratio assuming a C:P ratio in phytoplankton of 124 (Ho et al., 2003; Moore et al., 2013). The uncertainties associated with variable TM:C ratios are discussed in Section 4.2. The results of all flux calculations are listed in Table 1 and displayed in Figure 7.

3. Results

3.1 Biogeochemical conditions in the water column

The biogeochemical trends in the water column during our sampling campaign are presented in detail by Lüdke et al. (2020) and Plass et al. (2020). During the time of sampling, the bottom water above our sampling stations on the shelf was depleted in oxygen. The OMZ, with oxygen concentrations below the detection limit of the Winkler titration (3 to 5 µM), extended down to around 450 m water depth (Fig. 2). Within the OMZ, nitrogenous conditions prevailed and concentrations of nitrite were in excess of 4 µM between 150 and 300 m water depth.

3.2 Pore water data

Pore water concentrations of Mn were highest in the upper 5 to 10 cm of the sediment at most stations, reaching several hundreds of nanomoles per litre. In deeper sediments Mn concentrations dropped below 100 nM at Stations 1, 3 and 5 (75, 130 and 195 m). At all stations, higher concentrations in pore waters than in the overlying bottom waters were observed. This implies an upward-directed diffusive flux of Mn to the bottom water. Particularly sharp concentration gradients at the sediment-water interface (up to 420 nM cm^{-1}) were measured at the shallow shelf stations, which result in the highest diffusive flux at St. 1 (75 m) (-550 µmol m^{-2} y^{-1}). Diffusive Mn fluxes decreased with increasing water depth and the lowest value was observed at Station 9 (750 m) (-26 µmol m^{-2} y^{-1}).

Concentrations of Co in pore waters increased from the sediment surface towards deeper sediments by several nanomoles per litre at stations within the OMZ. Concentrations in the uppermost pore water sample (~ 1 nM) were higher than in overlying bottom waters (< 1 nM), which again implies an upward diffusive flux from the pore water to the bottom water. Diffusive fluxes ranged between -4.1 and -1.7 µmol m^{-2} y^{-1} on the shelf, whereas at St. 9 (750 m) the flux was lowest with -0.13 µmol m^{-2} y^{-1}.

Pore water Ni concentrations generally increased with increasing sediment depth at most shelf stations, from a few nanomoles per litre at the sediment surface up to 92 nM in deeper sediments at St. 6 (245 m). The highest pore water Ni concentrations were observed at Station 9 (750 m) (up to 365 nM). With the exception

of Station 4 (145 m), diffusive fluxes ranging from -12 to -71 µmol m^{-2} y^{-1} were directed from the pore water to the bottom water.

Copper concentrations were in the range of 2 to 26 nM and mostly varied around an average of 7 nM at stations within the OMZ. Concentration gradients across the sediment-water interface generally ranged between 2 and 10 nM cm^{-1} and diffusive fluxes were mostly directed out of the sediment (St. 1, 4, 5 and 9). The highest efflux of -3.5 µmol m^{-2} y^{-1} was observed at St. 9 (750 m). The highest flux into sediment was 13 µmol m^{-2} y^{-1} at St. 6.

The concentrations of dissolved Zn ranged between 20 and 40 nM at most stations and generally varied within a narrow range within the sediment cores. At a few stations, single values of maximum concentrations in the upper 10 cm reached close to or above 100 nM. Concentrations of Zn in bottom waters were of the order of several hundred nanomoles per litre. The high concentration gradients across the sediment-water interface imply downward diffusive fluxes of Zn into the sediment of up to 2000 µmol m^{-2} y^{-1} at St. 1 (75 m).

Concentrations of Cd in pore waters ranged between 0.1 and 2 nM. Bottom water concentrations were higher than concentrations in the surface pore water at most stations (St. 3, 4, 5 and 6) indicating a downward diffusive flux of 0.6 to 0.8 µmol m^{-2} y^{-1} into the sediment. Upward directed fluxes were observed at St. 1 (75 m) (-1.8 µmol m^{-2} y^{-1}) and St. 9 (750 m) (-0.3 µmol m^{-2} y^{-1}).

The sediment pore waters contained H_2S at all shelf stations. The highest concentrations (> 4000 µM) were measured at St. 1 (75 m). At St. 3 to 5 (130 to 195 m), concentrations reached up to 1000 µM. Hydrogen sulphide concentrations increased with sediment depth either from the sediment surface (St. 1 and 3) or from 5 cm depth (St. 4 and 5). At several stations, H_2S showed a peak between 5 and 15 cm (St. 1, 3, 4), whereas at St. 5 (195 m) the increase with depth was continuous. At the deepest station on the slope (St. 9), no H_2S was detected.

3.3 Total digestion data and trace metal excess

The total digestion data is presented together with the sequential extraction data in Fig. 4. Total sedimentary contents of Mn, Co and Zn generally decreased with distance offshore, whereas contents of Ni and Cd increased, except at St. 9 where Ni contents decreased and Cd contents were lowest. Sedimentary Cu contents were rather constant along the sampling transect. There were no large variations in total TM contents with increasing sediment depth. Average station values for the different TMs were between the following; Mn: 133 to 382 µg g^{-1}, Co: 3 to 8 µg g^{-1}, Ni: 22 to 104 µg g^{-1}, Cu: 58 to 46 µg g^{-1}, Zn: 98 to 178, Cd: 2 to 52 µg g^{-1}.

The calculated enrichment or depletion of the different TMs compared to the lithogenic background sedimentation off Peru (TM_{xs}) is displayed in Fig. 5. The negative TM_{xs} for Mn and Co illustrates that these TMs are depleted at all stations whereas Ni, Cu, Zn and Cd are enriched. These depletion and enrichment patterns as well as the ranges of TM_{xs} are similar to those observed in previous studies on the Peruvian margin (e.g. Böning et al., 2004; Little et al., 2015). Manganese showed the smallest depletion at the shallowest station St. 1 (75 m) (-56 µg g^{-1}) and the largest depletion at the deepest station St. 9 (750 m) (-138 µg g^{-1}). The depletion of Co (-4 to -6 µg g-1) varied across the transect and was smallest at St. 6 (245 m) and highest at St. 4 (145 m). Across the shelf, Ni_{xs} clearly increased (7 to 100 µg g^{-1}) whereas Cu_{xs} (33 to 40 µg g^{-1}) and Cd_{xs} (26 to 52 µg g^{-1}) increased only moderately with distance offshore. In contrast Zn_{xs} (74 to 124 µg g^{-1}) decreased across the shelf. The enrichment of Ni, Cu and Zn at the slope station (St. 9) was similar to those observed at the shelf stations, whereas Cd_{xs} was close to zero (2 µg g^{-1}).

3.4 Sequential extraction data

As pointed out in Section 2.2, multiple TM host phases may be dissolved in each step of the sequential extraction procedure (Huerta-Diaz and Morse, 1990; Zimmerman and Weindorf, 2010). Therefore, we refer to the extraction medium rather than specific target phases hereafter. The distribution of each TM across the different fractions was similar at all stations. The sum of the TM fractions mostly matched well with total TM contents obtained by total digestion (Fig. 4).

At all stations, the largest proportion (> 60 %) of sedimentary Mn and Co was present in the HF-fraction (i.e. as silicates). Most of the remaining Mn and Co was present in the combined HCl-fractions (i.e. as monosulphides, (oxyhydr)oxides, carbonates). Compared to Mn (2 to 6 %), a larger amount of Co (7 to 21 %) was present in the HNO_3-fraction (i.e. as pyrite or organic matter). Approximately half of the total sediment contents of Ni and Cu were present in the $HCl_{0.5M}$-fraction. The remaining Ni was contained in the HNO_3-fraction (30 %) and HCl_{1M}-fraction (20 %). The main host phase of Cu switched from the $HCl_{0.5M}$-fraction towards the HNO_3-fraction with increasing water depth. Similar to Ni and Cu, half of the total Zn content at the shelf stations was present in the $HCl_{0.5M}$-fraction. The remaining Zn was distributed among the HF-fraction (25 %), HCl_{1M}-fraction (20 %) and HNO_3-fraction (10 %). At St. 9 (750 m), most Zn was present in the HF-fraction (40 %). With the exception of Station 9, Cd was almost exclusively contained in the $HCl_{0.5M}$-fraction (95 %).

The combined HCl- and the HNO_3-extractions are plotted against TS and POC contents to help further constrain whether TMs in these host phases are likely to be associated with organic matter or sulphide minerals, respectively (Fig. 6). The data showed a negative correlation at the shelf stations (St. 1 to 6, 75 to 245 m) between POC and Mn, Co and Zn in the HCl-fraction (R^2 = 0.61, 0.56 and 0.36 respectively) and in the case of Mn also in the HNO_3-fraction (R^2 = 0.68) ($p < 0.001$). At the shelf stations, a positive correlation with POC was found for Ni in the HCl- and HNO_3-fractions (R^2 = 0.74 and 0.63 respectively, $p < 0.001$). A positive correlation of POC with Cu was also observed at the shelf stations in the HNO_3-fraction (R^2 = 0.75) and for Cd in the HCl-fraction (R^2 = 0.57) ($p < 0.001$). Most TMs showed no clear correlation with TS considering all shelf station data. However, in the HCl-fraction of the deeper Stations 5 to 9 (195 to 750 m), Cd, Ni, and Cu (R^2 = 0.93, 0.83 and 0.82 respectively, $p < 0.001$) and to a lesser extent Zn (R^2 = 0.46, $p = 0.001$) correlated with TS. If only St. 1 and 9 are considered, Co and Mn would fall on a line of linear regression in the HCl- (R^2 = 0.94 and 0.92 respectively) and in the HNO_3-fraction (R^2 = 0.77 and 0.71 respectively) ($p < 0.001$). If all stations are considered, Co still positively correlated with TS in the HNO_3-fraction (R^2 = 0.61, $p < 0.001$).

4. Discussion

4.1. Sedimentary depletion of manganese and cobalt

In line with other studies (Böning et al., 2004; Scholz et al., 2011; Little et al., 2015), our data showed depletion of Mn and Co in sediments on the Peruvian margin (Fig. 6). Excess fluxes of both TMs displayed a similar pattern of decreasing depletion along the transect and with distance from the coast (Mn: -1161 to -100 µmol m^{-2} y^{-1}, Co: -123 to -3.5 µmol m^{-2} y^{-1}) (Fig. 7). The depletion must be caused by a transfer of TMs from the solid phase to the dissolved phase and transport away from the study area. In anoxic sediments, Mn is commonly released from the solid phase to the sediment pore water through the reductive dissolution of Mn-oxides coupled to the remineralisation of organic matter (Canfield and Thamdrup, 2009). The sedimentary cycling of Mn and Co is often coupled, whereby Co delivery is generally associated with Mn-oxides. Dissolution of Mn-oxides thus also releases Co to pore waters under reducing conditions (Heggie and Lewis, 1984; Gendron et al., 1986; Sundby et al., 1986; Scholz and Neumann, 2007; van de Velde et al., 2020). However, our data are only partly consistent with a close coupling between the cycling of Mn and Co on the Peruvian shelf because the contribution of diffusive benthic efflux to the sedimentary depletion differs between the two TMs.

The diffusive Mn effluxes from the sediment pore water into the bottom water of 26 to 551 µmol m^{-2} y^{-1} determined from our sampling campaign may vary temporally as function of bottom water oxygen concentrations. The fluxes are remarkably similar to 5 to 460 µmol m^{-2} y^{-1} determined off Peru at 11°S in 2008 (Scholz et al., 2011), but orders-of-magnitude lower than values observed in less reducing continental margin systems (McManus et al., 2012) and restricted basins (Pakhomova et al., 2007; van de Velde et al., 2020). The diffusive fluxes agreed well with the overall sedimentary depletion at St. 4 (145 m) and 6 (245 m) (Fig. 7), demonstrating that loss by diffusion across the sediment-water interface can account for Mn depletion at these sites. At St. 1 (75 m), 3 (130 m) and 5 (195 m) only half of the depletion can be related to benthic efflux. Following previous studies (Landing and Bruland, 1987; Johnson et al., 1996; Noble et al., 2012), we argue that the remaining Mn dissolution takes place in the anoxic water column. Efficient offshore transport of the dissolved Mn liberated from particles in the water column and sediments (Vedamati et al., 2014) can explain

476 sedimentary Mn depletion and generally low benthic Mn fluxes compared to other
477 marine systems. At the slope station with oxic bottom water (St. 9, 750 m), Mn
478 depletion may be related to the particular sediment composition (phosphorite,
479 glauconite and lag sediment that generally contain less Mn) or to downslope transport
480 of Mn-depleted shelf sediment that has undergone extensive leaching prior to
481 deposition on the slope.

482 Few studies have reported diffusive benthic Co fluxes from sediments. The
483 effluxes of Co observed in our study were similar to those reported for sediments from
484 underneath oxygen-deficient bottom waters in the Santa Monica basin (around -4 µmol
485 m^{-2} y^{-1}) (Johnson et al., 1988). In contrast to Mn, however, these are far too low to
486 account for a substantial portion of the total depletion from the solid phase (up to -123
487 µmol m^{-2} y^{-1}). Particularly at St. 1 (75 m) and St. 3 (130 m), the diffusive efflux
488 accounted for less than 10 % of the total depletion (Fig. 7). As for Mn at St. 1, 3 and 5,
489 this implies that the bulk of particle-associated Co must have already dissolved in the
490 water column before reaching the seafloor.

491 The release of Co from particles in oxygen-deficient upwelling regions is
492 believed to play an important role in the Co budget of the upper ocean (Saito et al.,
493 2004; Noble et al., 2012). Model results suggest that the main external input flux of
494 dissolved Co to the ocean derives from sediments at continental margins, two thirds of
495 which is derived from sediments underneath oxygen-deficient bottom waters
496 (Tagliabue et al., 2018). By comparing Co:Al ratios in sediments off Peru to the ratio of
497 the lithogenic background, Hawco et al. (2016) calculated that around half of the land-
498 derived particulate Co is dissolved, which leads to the formation of a large Co plume
499 observed in the water column off Peru. This estimate agrees well with sedimentary
500 Co:Al ratios in our study. For comparison, Mn:Al ratios indicate that only 10 – 40 % of
501 land derived particulate Mn is ultimately lost from the sediments. Modelling studies
502 estimated Co fluxes from sediments off Peru of 25 µmol m^{-2} y^{-1} (Tagliabue et al., 2018).
503 The total depletion at the shelf stations 3, 4 and 5 (-27 to -12 µmol m^{-2} y^{-1}) is in good
504 agreement with this estimate. However, our findings reveal that < 5 µmol m^{-2} y^{-1} is
505 released from the sediments by diffusion whereas the majority of the Co is dissolved
506 in the water column.

507 The spatial decoupling between the release of Co and Mn may be explained by
508 a scenario where Co desorption from Mn oxide surfaces (Murray, 1975; Shaw et al.,

1990) happens more readily and prior to Mn oxide dissolution itself. An alternate explanation could be that upon release, Co chiefly remains in the dissolved phase whereas Mn undergoes partial re-precipitation in the water column and deposition at the seafloor. This mechanism may be particularly relevant at the shallow shelf (St. 1, 75 m) where the relative depletion of Co compared to Mn is higher (Co_{xs}:Mn_{xs} = 0.1) than further offshore (Co_{xs}:Mn_{xs} = 0.04) due to decreasing Mn:Al ratios (derived from Fig. 5). Consistent with this scenario, Mn oxidation has been shown to be faster than Co oxidation (Landing and Bruland, 1987; Tebo, 1991; Thamdrup et al., 1994; Moffett and Ho, 1996; Noble et al., 2012). Therefore, once released into the water column, there is little Co scavenging or removal (Noble et al., 2012; Hawco et al., 2016). Instead, Co concentrations in the water column are primarily controlled by phytoplankton uptake rather than co-precipitation with Mn (Saito et al., 2004).

Within the sediment pore water, a decoupling was observed between Mn and Co since dissolved Co:Mn ratios exceeded crustal and phytoplankton ratios and increased in a downcore direction (Fig. 8). Increasing Co:Mn ratios in pore water were related to decreasing Mn concentrations below a shallow maximum, which is attributed to the precipitation of Mn carbonate or Mn adsorption onto calcite (Middelburg et al., 1987; Kuleshov, 2017). Consistent with this notion, reactive Mn is mainly present in the HCl soluble fraction, which contains Mn carbonates, oxides and potentially some Mn bound to silicate minerals. In contrast to Mn, a significant proportion of sedimentary Co (7 to 21 %) was extracted with HNO_3 and Co concentrations within this fraction covaried with TS, which is mainly present as pyrite (Suits and Arthur, 2000; Scholz et al., 2014). This observation suggests that authigenic pyrite is an important burial phase for Co in Peru margin sediments. Overall, preferential precipitation and retention of Mn relative to Co in sediments on the shallow shelf is likely to contribute to increasing sedimentary Co to Mn contents along the transect (Fig. 4).

4.2 Sedimentary enrichment of nickel, copper, zinc and cadmium

The TMs Ni, Cu, Zn and Cd are enriched in sediments throughout the study area. Zinc is the only TM where diffusion across the sediment-water interface can explain the majority of TM accumulation (Fig. 7). By contrast, Ni, Cu and Cd must

primarily be supplied by particles. Nickel displays a negative diffusive flux out of the sediment indicating that a fraction of the particulate TM delivered is solubilised within the sediment and recycled into the bottom water. The various TM delivery pathways are discussed in the following sections.

4.2.1. Diffusive delivery of Zn

Based on a covariation between Zn enrichment factors and POC concentrations in sediments and elevated Zn concentrations in plankton, prior studies concluded that biological uptake and deposition of organic material represents the main delivery pathway of Zn to sediments on the Peruvian margin (Böning et al., 2004; Little et al., 2015). In contrast, our flux data reveal that this mechanism can only explain 10 to 20 % of the Zn accumulation on the shelf (60 to 2230 µmol m^{-2} y^{-1}) (Fig. 7). We find that molecular diffusion of Zn is the main process of Zn delivery to the sediments on the Peruvian margin. The diffusive flux of Zn into the sediment equals the total enrichment flux at St.1 (75 m) (around 2000 µmol m^{-2} $y^{-}1$) and the fluxes at the other shelf stations are high enough or even exceed the fluxes required to account for the excess Zn accumulation.

A steep Zn concentration gradient between the bottom water just above the sediment surface and pore waters was the driver for high diffusive fluxes (Fig. 3). Water column studies report Zn concentrations of only a few nanomoles (maximum10 nM) in open ocean waters (Bruland and Lohan, 2006; Conway and John, 2014, 2015b; Janssen and Cullen, 2015; Sieber et al., 2020) including those within the Peruvian OMZ (John et al., 2018; Rapp et al., 2020). However, only a few Zn concentration data for bottom waters are available. In bottom waters from benthic chamber incubations in productive coastal environments, Zn concentrations can reach several hundred nanomoles (Westerlund et al., 1986; Ciceri et al., 1992; Turetta et al., 2005), which is similar to the bottom water concentrations found in our study (23 to 780 nM) (Fig. 3). We suggest that the high Zn concentrations in bottom water are due to Zn release from labile organic matter within the benthic fluff layer overlying the sediment. In that case, organic material could still play a role in the delivery of easily dissolvable Zn to the seafloor. However, any Zn bound to organic material is unlikely to originate through

direct uptake from the photic zone as this flux is far lower compared to the diffusive flux. Instead, Zn scavenging by downward sinking organic material or Zn incorporation by pelagic microbial communities could be a viable mechanisms by which Zn is bound to organic molecules (Sheng et al., 2004; Vijayaraghavan et al., 2005; Ohnemus et al., 2017).

4.2.2 Particulate supply of Ni, Cu and Cd by organic matter or metal oxides

Particulate supply with phytoplankton-derived organic matter may contribute to the accumulation of Ni, Cu, and Cd in Peru margin sediments to a significant extent (Fig. 7). This is particularly the case for Ni, where uptake by phytoplankton and delivery to the seafloor could explain between 100 % (St. 1, 75 m) and 20 % (St. 5, 195 m) of the excess Ni accumulation at the shelf stations (87 to 180 µmol m^{-2} y^{-1}). A correlation between Ni and POC is typically found in sediments below OMZs in upwelling regions, including the sediments off Peru (Böning et al., 2015; Ciscato et al., 2018). It has been argued based on a correlation between concentrations of Ni and chlorine (an intermediate degradation product of chlorophyll pigments) in surface sediments off Peru that excess Ni is ultimately derived from enzymes within diatoms (Böning et al., 2015). A coupled supply of Ni and organic matter to the sediment is also supported by our sediment data. The station with the highest sedimentary Ni contents also showed the highest POC content (St. 6, 245 m) (Table S.4) and sequential extraction data of Ni correlated with POC contents in the HNO_3-fraction (Fig. 6).

In potential conflict with the above discussion, other studies have estimated that direct Ni uptake by phytoplankton and organic matter export can contribute only a fraction of the Ni_{xs} in Peru margin sediments (Little et al., 2015; Ciscato et al., 2018). This conclusion is based on a mismatch between the Ni enrichment factor and POC contents in Peruvian sediments compared to sediments below other oxygen depleted regions and higher Ni_{xs}:Zn_{xs} compared to plankton ratios (Little et al., 2015). Furthermore, Ciscato et al. (2018) found a mismatch between Ni:C and Ni:Si ratios in diatoms and Peru margin sediments. However, the Ni:C of sinking diatoms may be increased by preferential dissolution of POC or by Ni incorporation in reducing microniches within sinking organic matter, both of which would obscure Ni supply by

diatom remains (Ciscato et al., 2018). Furthermore, sedimentary organic carbon is subject to degradation (Dale et al., 2015b), biogenic silica undergoes dissolution (Dale et al., 2020) and Zn is delivered by molecular diffusion (see Section 4.2.1). Therefore, a match between Ni:C, Ni:Si and Ni:Zn in diatoms or plankton and sediments is not expected. We compensate for the mismatch between organic carbon delivery and sedimentary POC by considering POC rain rates rather than POC burial rates.

Our estimate of Ni delivery with organic material is still dependent on the Ni:C ratio within fresh biomass, which is applied in our calculations ($8.06 \cdot 10^{-6}$). Using a regional Ni:C ratio for diatoms ($3.7 \cdot 10^{-6}$) (Twining et al., 2011), POC-associated excess Ni would decrease by ~50 %. In contrast, applying the regional bulk plankton maximum ratio ($11.9 \cdot 0^{-6}$) (Twining et al., 2011), the excess delivery would increase by ~50 %. Another regional bulk plankton (mostly zooplankton) Ni:C ratio estimate ($9.15 \cdot 10^{-6}$) (Collier and Edmond, 1984) is similar to the value used in our calculation. Using the Ni:C ratio from particulate data off Peru ($3.71 \cdot 10^{-5}$), organic matter could supply between 80 to 100 % of Ni excess on the shelf. However, this ratio is derived from particles that are likely enriched in TMs by prokaryotic communities (Ohnemus et al., 2017). The Ni:POC ratio measured in bulk sediments off Peru (average $16 \cdot 10^{-5}$) were generally higher than the plankton ratios reported above (Fig. 9). However, the ratios in the uppermost surface sediment sample were closer to phytoplankton ratios than sedimentary ratios further downcore (surface Ni:POC = $8 \cdot 10^{-5}$ to $10 \cdot 10^{-5}$ at St. 3 to 6). This observation suggests that Ni is progressively enriched relative to C during degradation of organic matter and early diagenesis. Overall, our estimates suggest that biological Ni uptake and delivery with organic material make an important contribution to Ni accumulation in Peru margin sediments. However, determining the TM:C ratio in fresh local phytoplankton and zooplankton before alteration and in sinking biogenic particles near the seafloor would help to reduce the uncertainty of TM fluxes associated with organic matter on the Peruvian margin.

Some of the mismatch between Ni supply with organic matter and total Ni accumulation could be related to the delivery of other Ni-containing particulate phases such Mn- and Fe-oxides, which are known to scavenge Ni from the water column (Shaw et al., 1990; Audry et al., 2006; Little et al., 2015; Olson et al., 2017). The Ni content of the Mn-oxide birnessite has been shown to be as high as 40 mg g^{-1} (Peacock and Sherman, 2007). Especially at the deeper shelf stations, where Ni delivery with

organic material is less important (20 to 50 %), Ni delivery by Mn- and Fe-oxides could be important. Such a scenario is also supported by increasing Ni concentrations within the pore water of surface sediments, which coincides with the initial accumulation of dissolved Mn (and also of Fe) (Plass et al., 2020).

Only 16 to 36 % of the excess Cu accumulation (33 to 594 µmol m^{-2} y^{-1}) can be explained as direct uptake by phytoplankton (Fig. 7). The remainder must be delivered by another particulate phase. Pore water profiles of Cu and Cd (Fig. 3) do not provide evidence for major recycling processes within the surface sediment, which is why release of these elements from Mn- and Fe-oxides appears to be unlikely. However, it is known that Cu is quite reactive towards biogenic particles and scavenging by sinking biogenic material has been argued to be an important vector for Cu transfer from the water column to the sediment (Fischer et al., 1986; Johnson et al., 1988; Shaw et al., 1990; Sheng et al., 2004; Vance et al., 2008; Roshan and Wu, 2015; Little et al., 2017). Furthermore, the binding of Cu to organic matter is very stable and a decrease in bottom water oxygen concentrations has been shown to increase the association of Cu with organic matter (Fischer et al., 1986; Chakraborty et al., 2015, 2016). It therefore seems likely that the positive correlation between POC and Cu in the HNO_3-fraction (Fig. 6) is due to Cu association with organic matter, either in the water column or during early diagenesis. In suspended particles off Peru, Cu:C ratios ($2.9 \cdot 10^{-5}$) are elevated compared to phytoplankton and particulate Cu concentrations increase with water depth (Ohnemus et al., 2017; Lee et al., 2018). Using this elevated Cu:C ratio to calculate Cu delivery with organic matter yields a maximum estimate, which could explain the total Cu excess accumulation in shelf sediments. However, this ratio does not represent surface to mixed layer phytoplankton uptake (Ohnemus et al., 2017; Lee et al., 2018) but rather reflects the affinity of Cu to associate with sinking particles.

4.2.3 Precipitation of TM sulphide minerals within the water column or sediment

The TMs Cu, Zn and Cd are known to form their own sulphide minerals rather than to become incorporated into Fe sulphides such as mackinawite (FeS) and pyrite (FeS_2). Furthermore, their solubility in sulphidic water is low compared to Mn, Co and

Ni (Morse and Luther, 1999; Audry et al., 2006). It is thus likely that interaction with H_2S, either within the sediment or during sulphidic events in the water column, affects the mobility of Cu, Zn and Cd to some extent.

Cadmium sulphide (greenockite) has the lowest solubility among the TM sulphides that are relevant to this study. In the marine environment, greenockite precipitates at the presence of trace amounts of H_2S (Davies-Colley et al., 1985; Rosenthal et al., 1995). In a previous study, Plass et al. (2020) demonstrated based on benthic chamber incubation data that Cd sulphide precipitation in near bottom waters can quantitatively account for the majority (up to 60 %) of excess Cd accumulation on the Peruvian margin (24 to 260 µmol m^{-2} y^{-1}). Our new sequential extraction data provide additional evidence for the importance of Cd sulphide as a delivery and burial phase of Cd. At the shelf stations, Cd was exclusively present in the HCl-fraction at all sediment depths (Fig. 4) and Cd in the HCl-fraction correlated with TS (Fig. 5).

The behaviour of Cu in sulphidic environments is complex since multiple different Cu sulphide minerals, which may be dissolved in either HCl or HNO_3, exist (Morse and Luther, 1999). Furthermore, Cu may occur as Cu(I) or Cu(II) in these minerals and the conditions under which Cu reduction takes place is matter of debate (Pattrick et al., 1997; Theberge et al., 1997; Al-Farawati and van den Berg, 1999; Ehrlich et al., 2004; Goh et al., 2006). Copper forms sulphide complexes in anoxic waters, which are quite stable compared to other TM sulphide complexes (Dyrssen, 1988; Pattrick et al., 1997; Theberge et al., 1997; Al-Farawati and van den Berg, 1999). Experimental studies demonstrated that Cu sulphide complexes can be precipitated as covellite (CuS) from aqueous solutions (Luther et al., 2002). Therefore, a particulate Cu input via sulphide precipitation may contribute to the Cu enrichment in Peruvian sediments (cf. Ciscato et al., 2019). In particular at St. 1 (75 m), where the contribution of organic matter is rather low (< 3%) and pore waters were highly sulphidic, a possible release of H_2S into bottom water may have favoured Cu sulphide precipitation, in a similar manner as suggested for Cd. Ciscato et al. (2019) hypothesized that Cu sulphide precipitation in the water column and sediment is the main control on Cu delivery and retention in the Peru margin sediments. We cannot clearly distinguish between Cu bound to sulphide minerals or organic matter with our sequential extraction data. Given that we observed a positive correlation of Cu extracted with HNO_3 and

POC, Cu in this phase is likely related to organic matter rather than sulphide. However, Cu sulphides may be present within the HCl phase, in which a positive correlation with TS was observed (Fig. 6).

Unlike Cd (and maybe Cu), the precipitation of Zn sulphides (e.g., sphalerite) in the water column is not an important mechanism of Zn delivery to the seafloor. However, Zn sulphide precipitation within the sediment (Morse and Luther, 1999) is likely to be the ultimate reason for low Zn concentrations in pore water (< 5 nM) and downward diffusion of Zn from the bottom water. This notion is supported by our sequential extraction data showing that the majority of Zn in shelf sediments is present in the HCl-fraction (60 %), which contains ZnS (Fig. 4). By contrast, on the slope at St. 9 (750 m), where no H_2S was detected, Zn concentrations in pore waters are higher (up to 18 nM) and only 30 % of Zn is present in the HCl-fraction. Zinc removal from the anoxic water column has also been ascribed to Zn sulphide precipitation in particle microenvironments (Conway and John, 2015b; Janssen and Cullen, 2015). However, according to our data such a mechanism is not required to explain excess Zn accumulation in the sediment.

In contrast to Cu, Zn and Cd, Ni is unlikely to be delivered and/or buried as sulphide mineral on the Peruvian margin. In sulphidic marine environments, Ni is co-precipitated with pyrite and does not form its own sulphide minerals (Morse and Luther, 1999). Furthermore, Ni does not become precipitated from anoxic-sulphidic water columns (Tankéré et al., 2001). In agreement with a subordinate role of sulphides as a host phase for Ni in the sediment, Ni in both the HCl-fraction and the HNO_3-fraction correlated with POC rather than TS (Fig. 6).

5. Summary and conclusions

We presented TM data for sediments and pore waters along a latitudinal transect across the OMZ off Peru. Consistent with previous studies, our data reveal that sediments on the Peruvian shelf are a source of dissolved Mn and Co to the water column, whereas they represent a sink for dissolved Ni, Cu, Zn and Cd. We provided mass accumulation rates and diffusive benthic fluxes for each element, which can be used to better constrain trace metal fluxes in models and mass balances. Furthermore,

our data provide new insights into the pathways and main processes by which TMs are lost from or delivered to the sediment. Our findings are summarized in a schematic sketch shown in Figure 10:

1. Manganese and Co show a similar pattern of sedimentary depletion across the transect but the location where dissolution and liberation from particles takes place is different. While Mn is mostly solubilised in the sediment and lost to the water column by molecular diffusion across the sediment-water interface, the vast majority of Co is already liberated in the water column. Moreover, partial Mn retention in the sediment as Mn carbonates contributes to the decoupling of Mn and Co accumulation in Peruvian margin sediments.

2. Delivery of Ni to the sediment seems to be mostly mediated via Ni uptake by phytoplankton and downward sinking of organic material. In addition, scavenging of Ni by metal oxides in the water column may contribute to Ni accumulation in the sediment and some Ni recycling across the sediment-water interface as a result of metal oxide reduction.

3. Direct uptake of Cu, Zn and Cd by phytoplankton can explain only a minor fraction of the sedimentary accumulation of these TMs. Instead, Cu and Zn may become passively scavenged by organic material during downward sinking though the water column.

4. The majority of Zn accumulation is mediated by Zn sulphide precipitation in the sediment coupled to molecular diffusion of Zn across the sediment-water interface. High benthic Zn fluxes are primarily driven by high Zn concentrations in bottom waters, which are attributed to Zn liberation from labile organic matter within the fluffy layer overlying the sediment surface.

5. Cadmium delivery to the sediment surface is mediated by sulphide precipitation in the near-bottom water. A similar process may contribute to the particulate delivery of Cu to the sediment.

Our results demonstrate that bio-essential TMs are characterized by a complex and divergent behaviour under low-oxygen conditions. A decline in oceanic oxygen concentrations and an expansion of OMZs has been observed over the last decades (Stramma et al., 2010; Helm et al., 2011; Schmidtko et al., 2017) and is predicted to continue in the future (Bopp et al., 2002; Oschlies et al., 2008; Keeling et al., 2010).

According to our findings, TMs will respond differently to declining oxygen concentrations and the associated expansion of sulphidic conditions in surface sediments and bottom waters. While some TMs may be become increasingly released from particles or from the sediment into the water column (e.g. Mn, Co), others may be removed or retained in the sediments more efficiently (e.g. Ni, Cu, Zn, Cd). Ultimately, such different behaviour can modify the TM stoichiometry in upwelling water masses and potentially affect TM-dependent ecosystems in the surface ocean.

Acknowledgements

We are grateful for the support of the crew of RV Meteor during the fieldwork. For their technical and analytical assistance, we thank A. Bleyer, B. Domeyer, D. Jasinski, T. Steffens, and R. Surberg. This study was supported by the German Research Foundation through the Emmy Noether Nachwuchsforschergruppe ICONOX (Iron Cycling in Continental Margin Sediments and the Nutrient and Oxygen Balance of the Ocean) and Sonderforschungsbereich 754 (Climate-Biogeochemistry Interactions in the Tropical Ocean). We would also like to thank S. H. Little and one anonymous reviewer for their constructive comments and thoughtful questions which helped to improve this manuscript, as well as T. S. Bianchi and P. H. Santschi for the editorial handling.

References

Aguirre, L., 1988. Chemical mobility during low-grade metamorphism of a Jurassic lava flow: Río Grande Formation, Peru. J. South Am. Earth Sci. 1, 343–361. https://doi.org/10.1016/0895-9811(88)90022-3

Al-Farawati, R., van den Berg, C.M.G., 1999. Metal–sulfide complexation in seawater. Mar. Chem. 63, 331–352. https://doi.org/10.1016/S0304-4203(98)00056-5

Algeo, T.J., Liu, J., 2020. A re-assessment of elemental proxies for paleoredox

797 analysis. Chem. Geol. 540, 119549.
798 https://doi.org/10.1016/j.chemgeo.2020.119549

799 Archer, C., Vance, D., Milne, A., Lohan, M.C., 2020. The oceanic biogeochemistry of
800 nickel and its isotopes: New data from the South Atlantic and the Southern
801 Ocean biogeochemical divide. Earth Planet. Sci. Lett. 535, 116118.
802 https://doi.org/10.1016/j.epsl.2020.116118

803 Audry, S., Blanc, G., Schäfer, J., Chaillou, G., Robert, S., 2006. Early diagenesis of
804 trace metals (Cd, Cu, Co, Ni, U, Mo, and V) in the freshwater reaches of a
805 macrotidal estuary. Geochim. Cosmochim. Acta 70, 2264–2282.
806 https://doi.org/10.1016/j.gca.2006.02.001

807 Baeyens, W., Monteny, F., Leermakers, M., Bouillon, S., 2003. Evalution of
808 sequential extractions on dry and wet sediments. Anal. Bioanal. Chem. 376,
809 890–901. https://doi.org/10.1007/s00216-003-2005-z

810 Böning, P., Brumsack, H.J., Böttcher, M.E., Schnetger, B., Kriete, C., Kallmeyer, J.,
811 Borchers, S.L., 2004. Geochemistry of Peruvian near-surface sediments.
812 Geochim. Cosmochim. Acta 68, 4429–4451.
813 https://doi.org/10.1016/j.gca.2004.04.027

814 Böning, P., Brumsack, H.J., Schnetger, B., Grunwald, M., 2009. Trace element
815 signatures of Chilean upwelling sediments at ~ 36°S. Mar. Geol. 259, 112–121.
816 https://doi.org/10.1016/j.margeo.2009.01.004

817 Böning, P., Shaw, T., Pahnke, K., Brumsack, H.-J., 2015. Nickel as indicator of fresh
818 organic matter in upwelling sediments. Geochim. Cosmochim. Acta 162, 99–108.
819 https://doi.org/10.1016/j.gca.2015.04.027

820 Bopp, L., Le Quéré, C., Heimann, M., Manning, A.C., Monfray, P., 2002. Climate-
821 induced oceanic oxygen fluxes: Implications for the contemporary carbon
822 budget. Global Biogeochem. Cycles 16, 6-1-6–13.
823 https://doi.org/10.1029/2001GB001445

824 Borchers, S.L., Schnetger, B., Böning, P., Brumsack, H.-J., 2005. Geochemical
825 signatures of the Namibian diatom belt: Perennial upwelling and intermittent
826 anoxia. Geochemistry, Geophys. Geosystems 6.
827 https://doi.org/10.1029/2004GC000886

828 Boudreau, B.P., 1997. Diagenetic Models and Their Implementation. Springer.
829 https://doi.org/10.1007/978-3-642-60421-8

830 Bruland, K.W., Lohan, M.C., 2006. Controls of Trace Metals in Seawater, in:
831 Elderfield, H. (Ed.), The Oceans and Marine Geochemistry, Treatise on
832 Geochemistry. Elsevier, pp. 23–47.

833 Brumsack, H.J., 2006. The trace metal content of recent organic carbon-rich
834 sediments: Implications for Cretaceous black shale formation. Palaeogeogr.
835 Palaeoclimatol. Palaeoecol. 232, 344–361.
836 https://doi.org/10.1016/j.palaeo.2005.05.011

837 Canfield, D.E., Thamdrup, B., 2009. Towards a consistent classification scheme for
838 geochemical environments, or, why we wish the term “suboxic” would go away:
839 Editorial. Geobiology 7, 385–392. https://doi.org/10.1111/j.1472-
840 4669.2009.00214.x

841 Chakraborty, P., Ramteke, D., Chakraborty, S., 2015. Geochemical partitioning of Cu
842 and Ni in mangrove sediments: Relationships with their bioavailability. Mar.
843 Pollut. Bull. 93, 194–201. https://doi.org/10.1016/j.marpolbul.2015.01.016

844 Chakraborty, P., Chakraborty, S., Jayachandran, S., Madan, R., Sarkar, A., Linsy, P.,
845 Nath, B.N., 2016. Effects of bottom water dissolved oxygen variability on copper
846 and lead fractionation in the sediments across the oxygen minimum zone,
847 western continental margin of India. Sci. Total Environ. 566–567, 1052–1061.
848 https://doi.org/10.1016/j.scitotenv.2016.05.125

849 Ciceri, G., Maran, C., Martinotti, W., Queirazza, G., 1992. Geochemical cycling of
850 heavy metals in a marine coastal area: benthic flux determination from pore
851 water profiles and in situ measurements using benthic chambers. Hydrobiologia
852 235–236, 501–517. https://doi.org/10.1007/BF00026238

853 Ciscato, E.R., Bontognali, T.R.R., Vance, D., 2018. Nickel and its isotopes in organic-
854 rich sediments: implications for oceanic budgets and a potential record of ancient
855 seawater. Earth Planet. Sci. Lett. 494, 239–250.
856 https://doi.org/10.1016/j.epsl.2018.04.061

857 Ciscato, E.R., Bontognali, T.R.R., Poulton, S.W., Vance, D., 2019. Copper and its
858 Isotopes in Organic-Rich Sediments: From the Modern Peru Margin to Archean

Shales. Geosciences 9, 325. https://doi.org/10.3390/geosciences9080325

Collier, R., Edmond, J., 1984. The trace element geochemistry of marine biogenic particulate matter. Prog. Oceanogr. 13, 113–199. https://doi.org/10.1016/0079-6611(84)90008-9

Conway, T.M., John, S.G., 2014. The biogeochemical cycling of zinc and zinc isotopes in the North Atlantic Ocean. Global Biogeochem. Cycles 28, 1111–1128. https://doi.org/10.1002/2014GB004862

Conway, T.M., John, S.G., 2015a. Biogeochemical cycling of cadmium isotopes along a high-resolution section through the North Atlantic Ocean. Geochim. Cosmochim. Acta 148, 269–283. https://doi.org/10.1016/j.gca.2014.09.032

Conway, T.M., John, S.G., 2015b. The cycling of iron, zinc and cadmium in the North East Pacific Ocean - Insights from stable isotopes. Geochim. Cosmochim. Acta 164, 262–283. https://doi.org/10.1016/j.gca.2015.05.023

Dale, A.W., Nickelsen, L., Scholz, F., Hensen, C., Oschlies, A., Wallmann, K., 2015a. A revised global estimate of dissolved iron fluxes from marine sediments. Global Biogeochem. Cycles 29, 691–707. https://doi.org/10.1002/2014GB005017

Dale, A.W., Sommer, S., Lomnitz, U., Montes, I., Treude, T., Liebetrau, V., Gier, J., Hensen, C., Dengler, M., Stolpovsky, K., Bryant, L.D., Wallmann, K., 2015b. Organic carbon production, mineralisation and preservation on the Peruvian margin. Biogeosciences 12, 1537–1559. https://doi.org/10.5194/bg-12-1537-2015

Dale, A.W., Paul, M., Clemens, D., Scholz, F., Schroller- Lomnitz, U., Wallmann, K., Geilert, S., Hensen, C., Plass, A., Liebetrau, V., Grasse, P., Sommer, S., 2020. Recycling and burial of biogenic silica in an open margin oxygen minimum zone. Global Biogeochem. Cycles. https://doi.org/10.1029/2020GB006583

Davies-Colley, R.J., Nelson, P.O., Williamson, K.J., 1985. Sulfide control of cadmium and copper concentrations in anaerobic estuarine sediments. Mar. Chem. 16, 173–186. https://doi.org/10.1016/0304-4203(85)90021-0

Dyrssen, D., 1988. Sulfide complexation in surface seawater. Mar. Chem. 24, 143–153. https://doi.org/10.1016/0304-4203(88)90045-X

889 Echevin, V., Aumont, O., Ledesma, J., Flores, G., 2008. The seasonal cycle of
890 surface chlorophyll in the Peruvian upwelling system: A modelling study. Prog.
891 Oceanogr. 79, 167–176. https://doi.org/10.1016/j.pocean.2008.10.026

892 Ehrlich, S., Butler, I., Halicz, L., Rickard, D., Oldroyd, A., Matthews, A., 2004.
893 Experimental study of the copper isotope fractionation between aqueous Cu(II)
894 and covellite, CuS. Chem. Geol. 209, 259–269.
895 https://doi.org/10.1016/j.chemgeo.2004.06.010

896 Fischer, K., Dymond, J., Lyle, M., Soutar, A., Rau, S., 1986. The benthic cycle of
897 copper: Evidence from sediment trap experiments in the eastern tropical North
898 Pacific Ocean. Geochim. Cosmochim. Acta 50, 1535–1543.
899 https://doi.org/10.1016/0016-7037(86)90327-3

900 Freund, M., 2020. Dispersion of a Tracer in the Eastern Tropical South Pacific - an
901 Investigation of Interactions from the Benthic Boundary Layer to the Ocean
902 Interior -. Dr. Diss.

903 Froelich, P.., Arthur, M.., Burnett, W.., Deakin, M., Hensley, V., Jahnke, R., Kaul, L.,
904 Kim, K.-H., Roe, K., Soutar, A., Vathakanon, C., 1988. Early diagenesis of
905 organic matter in Peru continental margin sediments: Phosphorite precipitation.
906 Mar. Geol. 80, 309–343. https://doi.org/10.1016/0025-3227(88)90095-3

907 Gendron, A., Silverberg, N., Sundby, B., Lebel, J., 1986. Early diagenesis of
908 cadmium and cobalt in sediments of the Laurentian Trough. Geochim.
909 Cosmochim. Acta 50, 741–747.
910 https://doi.org/10.1016/j.ijmachtools.2007.10.013

911 Goh, S.W., Buckley, A.N., Lamb, R.N., 2006. Copper(II) sulfide? Miner. Eng. 19,
912 204–208. https://doi.org/10.1016/j.mineng.2005.09.003

913 Grasshoff, M., Erhardt, M., Kremling, K., 1999. Methods of seawater analysis. Wiley-
914 VCH, Weinheim. https://doi.org/10.1002/ange.19770890738

915 Gutiérrez, D., Enríquez, E., Purca, S., Quipúzcoa, L., Marquina, R., Flores, G.,
916 Graco, M., 2008. Oxygenation episodes on the continental shelf of central Peru:
917 Remote forcing and benthic ecosystem response. Prog. Oceanogr. 79, 177–189.
918 https://doi.org/10.1016/j.pocean.2008.10.025

919 Hawco, N.J., Ohnemus, D.C., Resing, J.A., Twining, B.S., Saito, M.A., 2016. A

dissolved cobalt plume in the oxygen minimum zone of the eastern tropical South Pacific. Biogeosciences 13, 5697–5717. https://doi.org/10.5194/bg-13-5697-2016

Heggie, D., Lewis, T., 1984. Cobalt in pore waters of marine sediments. Nature 311, 453–455. https://doi.org/10.1038/311453a0

Helm, K.P., Bindoff, N.L., Church, J.A., 2011. Observed decreases in oxygen content of the global ocean. Geophys. Res. Lett. 38, 1–6. https://doi.org/10.1029/2011GL049513

Ho, T.-Y., Quigg, A., Finkel, Z. V., Milligan, A.J., Wyman, K., Falkowski, P.G., Morel, F.M.M., 2003. THE ELEMENTAL COMPOSITION OF SOME MARINE PHYTOPLANKTON1. J. Phycol. 39, 1145–1159. https://doi.org/10.1111/j.0022-3646.2003.03-090.x

Homoky, W.B., Weber, T., Berelson, W.M., Conway, T.M., Henderson, G.M., van Hulten, M., Jeandel, C., Severmann, S., Tagliabue, A., 2016. Quantifying trace element and isotope fluxes at the ocean–sediment boundary: a review. Philos. Trans. R. Soc. A Math. Phys. Eng. Sci. 374, 20160246. https://doi.org/10.1098/rsta.2016.0246

Huerta-Diaz, M.A., Morse, J.W., 1990. A quantitative method for determination of trace metal concentrations in sedimentary pyrite. Mar. Chem. 29, 119–144. https://doi.org/10.1016/0304-4203(90)90009-2

Jacobs, L., Emerson, S., Skei, J., 1985. Partitioning and transport of metals across the O2 H2S interface in a permanently anoxic basin: Framvaren Fjord, Norway. Geochim. Cosmochim. Acta 49, 1433–1444. https://doi.org/10.1016/0016-7037(85)90293-5

Janssen, D.J., Conway, T.M., John, S.G., Christian, J.R., Kramer, D.I., Pedersen, T.F., Cullen, J.T., 2014. Undocumented water column sink for cadmium in open ocean oxygen-deficient zones. Proc. Natl. Acad. Sci. 111, 6888–6893. https://doi.org/10.1073/pnas.1402388111

Janssen, D.J., Cullen, J.T., 2015. Decoupling of zinc and silicic acid in the subarctic northeast Pacific interior. Mar. Chem. 177, 124–133. https://doi.org/10.1016/j.marchem.2015.03.014

John, S.G., Helgoe, J., Townsend, E., Weber, T., DeVries, T., Tagliabue, A., Moore, K., Lam, P., Marsay, C.M., Till, C., 2018. Biogeochemical cycling of Fe and Fe stable isotopes in the Eastern Tropical South Pacific. Mar. Chem. 201, 66–76. https://doi.org/10.1016/j.marchem.2017.06.003

Johnson, K.S., Stout, P.M., Berelson, W.M., Sakamoto-Arnold, C.M., 1988. Cobalt and copper distributions in the waters of Santa Monica Basin, California. Nature 332, 527–530. https://doi.org/10.1038/332527a0

Johnson, K.S., Coale, K.H., Berelson, W.M., Michael Gordon, R., 1996. On the formation of the manganese maximum in the oxygen minimum. Geochim. Cosmochim. Acta 60, 1291–1299. https://doi.org/10.1016/0016-7037(96)00005-1

Karstensen, J., Stramma, L., Visbeck, M., 2008. Oxygen minimum zones in the eastern tropical Atlantic and Pacific oceans. Prog. Oceanogr. 77, 331–350. https://doi.org/10.1016/j.pocean.2007.05.009

Keeling, R.F., Körtzinger, A., Gruber, N., 2010. Ocean Deoxygenation in a Warming World. Ann. Rev. Mar. Sci. 2, 199–229. https://doi.org/10.1146/annurev.marine.010908.163855

Kostka, J.E., Luther, G.W., 1994. Partitioning and speciation of solid phase iron in saltmarsh sediments. Geochim. Cosmochim. Acta 58, 1701–1710. https://doi.org/10.1016/0016-7037(94)90531-2

Kuleshov, V., 2017. Manganese Carbonates in Modern Sediments, in: Isotope Geochemistry. Elsevier, pp. 5–62. https://doi.org/10.1016/B978-0-12-803165-0.00002-1

Landing, W.M., Bruland, K.W., 1987. The contrasting biogeochemistry of iron and manganese in the Pacific Ocean. Geochim. Cosmochim. Acta 51, 29–43. https://doi.org/10.1016/0016-7037(87)90004-4

Lee, J.-M., Heller, M.I., Lam, P.J., 2018. Size distribution of particulate trace elements in the U.S. GEOTRACES Eastern Pacific Zonal Transect (GP16). Mar. Chem. 201, 108–123. https://doi.org/10.1016/j.marchem.2017.09.006

Levin, L., Gutiérrez, D., Rathburn, A., Neira, C., Sellanes, J., Muñoz, P., Gallardo, V., Salamanca, M., 2002. Benthic processes on the Peru margin: a transect across

982 the oxygen minimum zone during the 1997–98 El Niño. Prog. Oceanogr. 53, 1–
983 27. https://doi.org/10.1016/S0079-6611(02)00022-8

984 Li, Y.-H., Gregory, S., 1974. Diffusion of ions in sea water and in deep-sea
985 sediments. Geochim. Cosmochim. Acta 38, 703–714.
986 https://doi.org/10.1016/0016-7037(74)90145-8

987 Little, S.H., Vance, D., Lyons, T.W., McManus, J., 2015. Controls on trace metal
988 authigenic enrichment in reducing sediments: Insights from modern oxygen-
989 deficient settings. Am. J. Sci. 315, 77–119. https://doi.org/10.2475/02.2015.01

990 Little, S.H., Vance, D., McManus, J., Severmann, S., 2016. Key role of continental
991 margin sediments in the oceanic mass balance of Zn and Zn isotopes. Geology
992 44, 207–210. https://doi.org/10.1130/G37493.1

993 Little, S.H., Vance, D., McManus, J., Severmann, S., Lyons, T.W., 2017. Copper
994 isotope signatures in modern marine sediments. Geochim. Cosmochim. Acta
995 212, 253–273. https://doi.org/10.1016/j.gca.2017.06.019

996 Lohan, M.C., Tagliabue, A., 2018. Oceanic Micronutrients: Trace Metals that are
997 Essential for Marine Life. Elements 14, 385–390.
998 https://doi.org/10.2138/gselements.14.6.385

999 Lüdke, J., Dengler, M., Sommer, S., Clemens, D., Thomsen, S., Krahmann, G., Dale,
1000 A.W., Achterberg, E.P., Visbeck, M., 2020. Influence of intraseasonal eastern
1001 boundary circulation variability on hydrography and biogeochemistry off Peru.
1002 Ocean Sci. 16, 1347–1366. https://doi.org/10.5194/os-16-1347-2020

1003 Luther, G.W., Theberge, S.M., Rozan, T.F., Rickard, D., Rowlands, C.C., Oldroyd, A.,
1004 2002. Aqueous Copper Sulfide Clusters as Intermediates during Copper Sulfide
1005 Formation. Environ. Sci. Technol. 36, 394–402.
1006 https://doi.org/10.1021/es010906k

1007 McManus, J., Berelson, W.M., Severmann, S., Johnson, K.S., Hammond, D.E., Roy,
1008 M., Coale, K.H., 2012. Benthic manganese fluxes along the Oregon–California
1009 continental shelf and slope. Cont. Shelf Res. 43, 71–85.
1010 https://doi.org/10.1016/j.csr.2012.04.016

1011 Middelburg, J.J., De Lange, G.J., van Der Weijden, C.H., 1987. Manganese solubility
1012 control in marine pore waters. Geochim. Cosmochim. Acta 51, 759–763.

https://doi.org/10.1016/0016-7037(87)90086-X

Moffett, J.W., Ho, J., 1996. Oxidation of cobalt and manganese in seawater via a common microbially catalyzed pathway. Geochim. Cosmochim. Acta 60, 3415–3424. https://doi.org/10.1016/0016-7037(96)00176-7

Moore, C.M., Mills, M.M., Arrigo, K.R., Berman-Frank, I., Bopp, L., Boyd, P.W., Galbraith, E.D., Geider, R.J., Guieu, C., Jaccard, S.L., Jickells, T.D., La Roche, J., Lenton, T.M., Mahowald, N.M., Marañón, E., Marinov, I., Moore, J.K., Nakatsuka, T., Oschlies, A., Saito, M.A., Thingstad, T.F., Tsuda, A., Ulloa, O., 2013. Processes and patterns of oceanic nutrient limitation. Nat. Geosci. 6, 701–710. https://doi.org/10.1038/ngeo1765

Morel, F.M.M., Price, N.M., 2003. The Biogeochemical Cycles of Trace Metals in the Oceans. Science (80-.). 300, 944–947. https://doi.org/10.1126/science.1083545

Morel, F.M.M., Milligan, A.J., Saito, M.A., 2014. Marine Bioinorganic Chemistry: The Role of Trace Metals in the Oceanic Cycles of Major Nutrients, in: Treatise on Geochemistry. Elsevier, pp. 123–150. https://doi.org/10.1016/B978-0-08-095975-7.00605-7

Morford, J.L., Emerson, S., 1999. The geochemistry of redox sensitive trace metals in sediments. Geochim. Cosmochim. Acta 63, 1735–1750. https://doi.org/10.1016/S0016-7037(99)00126-X

Morse, J.W., Luther, G.W., 1999. Chemical influences on trace metal-sulfide interactions in anoxic sediments. Geochim. Cosmochim. Acta 63, 3373–3378. https://doi.org/10.1016/S0016-7037(99)00258-6

Muñoz, P., Lange, C.B., Gutiérrez, D., Hebbeln, D., Salamanca, M.A., Dezileau, L., Reyss, J.L., Benninger, L.K., 2004. Recent sedimentation and mass accumulation rates based on 210Pb along the Peru–Chile continental margin. Deep Sea Res. Part II Top. Stud. Oceanogr. 51, 2523–2541. https://doi.org/10.1016/j.dsr2.2004.08.015

Murray, J.W., 1975. The interaction of cobalt with hydrous manganese dioxide. Geochim. Cosmochim. Acta 39, 635–647. https://doi.org/10.1016/0016-7037(75)90007-1

Nameroff, T.J., Balistrieri, L.S., Murray, J.W., 2002. Suboxic trace metal

geochemistry in the Eastern Tropical North Pacific. Geochim. Cosmochim. Acta 66, 1139–1158. https://doi.org/10.1016/S0016-7037(01)00843-2

Noble, A.E., Lamborg, C.H., Ohnemus, D.C., Lam, P.J., Goepfert, T.J., Measures, C.I., Frame, C.H., Casciotti, K.L., DiTullio, G.R., Jennings, J., Saito, M.A., 2012. Basin-scale inputs of cobalt, iron, and manganese from the Benguela-Angola front to the South Atlantic Ocean. Limnol. Oceanogr. 57, 989–1010. https://doi.org/10.4319/lo.2012.57.4.0989

Noffke, A., Hensen, C., Sommer, S., Scholz, F., Bohlen, L., Mosch, T., Graco, M., Wallmann, K., 2012. Benthic iron and phosphorus fluxes across the Peruvian oxygen minimum zone. Limnol. Oceanogr. 57, 851–867. https://doi.org/10.4319/lo.2012.57.3.0851

Ohde, T., 2018. Coastal Sulfur Plumes off Peru During El Niño, La Niña, and Neutral Phases. Geophys. Res. Lett. 45, 7075–7083. https://doi.org/10.1029/2018GL077618

Ohnemus, D.C., Rauschenberg, S., Cutter, G.A., Fitzsimmons, J.N., Sherrell, R.M., Twining, B.S., 2017. Elevated trace metal content of prokaryotic communities associated with marine oxygen deficient zones. Limnol. Oceanogr. 62, 3–25. https://doi.org/10.1002/lno.10363

Olson, L., Quinn, K.A., Siebecker, M.G., Luther, G.W., Hastings, D., Morford, J.L., 2017. Trace metal diagenesis in sulfidic sediments: Insights from Chesapeake Bay. Chem. Geol. 452, 47–59. https://doi.org/10.1016/j.chemgeo.2017.01.018

Oschlies, A., Schulz, K.G., Riebesell, U., Schmittner, A., 2008. Simulated 21st century's increase in oceanic suboxia by CO 2-enhanced biotic carbon export. Global Biogeochem. Cycles 22, 1–10. https://doi.org/10.1029/2007GB003147

Pakhomova, S. V., Hall, P.O.J., Kononets, M.Y., Rozanov, A.G., Tengberg, A., Vershinin, A. V., 2007. Fluxes of iron and manganese across the sediment–water interface under various redox conditions. Mar. Chem. 107, 319–331. https://doi.org/10.1016/j.marchem.2007.06.001

Pattrick, R.A.D., Mosselmans, J.F.W., Charnock, J.M., England, K.E.R., Helz, G.R., Garner, C.D., Vaughan, D.J., 1997. The structure of amorphous copper sulfide precipitates: An X-ray absorption study. Geochim. Cosmochim. Acta 61, 2023–

2036. https://doi.org/10.1016/S0016-7037(97)00061-6

Peacock, C.L., Sherman, D.M., 2007. Sorption of Ni by birnessite: Equilibrium controls on Ni in seawater. Chem. Geol. 238, 94–106. https://doi.org/10.1016/j.chemgeo.2006.10.019

Pennington, J.T., Mahoney, K.L., Kuwahara, V.S., Kolber, D.D., Calienes, R., Chavez, F.P., 2006. Primary production in the eastern tropical Pacific: A review. Prog. Oceanogr. 69, 285–317. https://doi.org/10.1016/j.pocean.2006.03.012

Plass, A., Schlosser, C., Sommer, S., Dale, A.W., Achterberg, E.P., Scholz, F., 2020. The control of hydrogen sulfide on benthic iron and cadmium fluxes in the oxygen minimum zone off Peru. Biogeosciences 17, 3685–3704. https://doi.org/10.5194/bg-17-3685-2020

Rapp, I., Schlosser, C., Rusiecka, D., Gledhill, M., Achterberg, E.P., 2017. Automated preconcentration of Fe, Zn, Cu, Ni, Cd, Pb, Co, and Mn in seawater with analysis using high-resolution sector field inductively-coupled plasma mass spectrometry. Anal. Chim. Acta 976, 1–13. https://doi.org/10.1016/j.aca.2017.05.008

Rapp, I., Schlosser, C., Menzel Barraqueta, J.-L., Wenzel, B., Lüdke, J., Scholten, J., Gasser, B., Reichert, P., Gledhill, M., Dengler, M., Achterberg, E.P., 2019. Controls on redox-sensitive trace metals in the Mauritanian oxygen minimum zone. Biogeosciences 16, 4157–4182. https://doi.org/10.5194/bg-16-4157-2019

Rapp, I., Schlosser, C., Browning, T.J., Wolf, F., Le Moigne, F.A.C., Gledhill, M., Achterberg, E.P., 2020. El Niño-Driven Oxygenation Impacts Peruvian Shelf Iron Supply to the South Pacific Ocean. Geophys. Res. Lett. 47. https://doi.org/10.1029/2019GL086631

Reimers, C.E., Suess, E., 1983. Spatial and Temporal Patterns of Organic Matter Accumulation on the Peru Continental Margin. NATO Conf. Ser. 4 Mar. Sci. 10 B, 311–345.

Rigaud, S., Radakovitch, O., Couture, R.M., Deflandre, B., Cossa, D., Garnier, C., Garnier, J.M., 2013. Mobility and fluxes of trace elements and nutrients at the sediment-water interface of a lagoon under contrasting water column oxygenation conditions. Appl. Geochemistry 31, 35–51.

https://doi.org/10.1016/j.apgeochem.2012.12.003

Rosenthal, Y., Lam, P., Boyle, E.A., Thomson, J., 1995. Precipitation and postdepositional mobility. Earth Planet. Sci. Lett. 132, 99–111. https://doi.org/10.1016/0012-821X(95)00056-I

Roshan, S., Wu, J., 2015. The distribution of dissolved copper in the tropical-subtropical north Atlantic across the GEOTRACES GA03 transect. Mar. Chem. 176, 189–198. https://doi.org/10.1016/j.marchem.2015.09.006

Saito, M.A., Moffett, J.W., DiTullio, G.R., 2004. Cobalt and nickel in the Peru upwelling region: A major flux of labile cobalt utilized as a micronutrient. Global Biogeochem. Cycles 18, 1–14. https://doi.org/10.1029/2003GB002216

Saito, M.A., Goepfert, T.J., Ritt, J.T., 2008. Some thoughts on the concept of colimitation: Three definitions and the importance of bioavailability. Limnol. Oceanogr. 53, 276–290. https://doi.org/10.4319/lo.2008.53.1.0276

Sarbas, B., Nohl, U., 2009. The GEOROC database – a decade of “online geochemistry.” Geochim. Cosmochim. Acta 73, Supplement p. A1158.

Schmidtko, S., Stramma, L., Visbeck, M., 2017. Decline in global oceanic oxygen content during the past five decades. Nature 542, 335–339. https://doi.org/10.1038/nature21399

Scholz, F., Neumann, T., 2007. Trace element diagenesis in pyrite-rich sediments of the Achterwasser lagoon, SW Baltic Sea. Mar. Chem. 107, 516–532. https://doi.org/10.1016/j.marchem.2007.08.005

Scholz, F., Hensen, C., Noffke, A., Rohde, A., Liebetrau, V., Wallmann, K., 2011. Early diagenesis of redox-sensitive trace metals in the Peru upwelling area - response to ENSO-related oxygen fluctuations in the water column. Geochim. Cosmochim. Acta 75, 7257–7276. https://doi.org/10.1016/j.gca.2011.08.007

Scholz, F., Severmann, S., McManus, J., Noffke, A., Lomnitz, U., Hensen, C., 2014. On the isotope composition of reactive iron in marine sediments: Redox shuttle versus 45 early diagenesis. Chem. Geol. 389, 48–59. https://doi.org/10.1016/j.chemgeo.2014.09.009

Scholz, F., Löscher, C.R., Fiskal, A., Sommer, S., Hensen, C., Lomnitz, U., Wuttig,

1136 K., Göttlicher, J., Kossel, E., Steininger, R., Canfield, D.E., 2016. Nitrate-
1137 dependent iron oxidation limits iron transport in anoxic ocean regions. Earth
1138 Planet. Sci. Lett. 454, 272–281. https://doi.org/10.1016/j.epsl.2016.09.025

1139 Schunck, H., Lavik, G., Desai, D.K., Großkopf, T., Kalvelage, T., Löscher, C.R.,
1140 Paulmier, A., Contreras, S., Siegel, H., Holtappels, M., Rosenstiel, P.,
1141 Schilhabel, M.B., Graco, M., Schmitz, R.A., Kuypers, M.M.M., LaRoche, J.,
1142 2013. Giant Hydrogen Sulfide Plume in the Oxygen Minimum Zone off Peru
1143 Supports Chemolithoautotrophy. PLoS One 8.
1144 https://doi.org/10.1371/journal.pone.0068661

1145 Shaw, T.J., Gieskes, J.M., Jahnke, R.A., 1990. Early diagenesis in differing
1146 depositional environments: The response of transition metals in pore water.
1147 Geochim. Cosmochim. Acta 54, 1233–1246. https://doi.org/10.1016/0016-
1148 7037(90)90149-F

1149 Sheng, P.X., Ting, Y.-P., Chen, J.P., Hong, L., 2004. Sorption of lead, copper,
1150 cadmium, zinc, and nickel by marine algal biomass: characterization of
1151 biosorptive capacity and investigation of mechanisms. J. Colloid Interface Sci.
1152 275, 131–141. https://doi.org/10.1016/j.jcis.2004.01.036

1153 Sieber, M., Conway, T.M., de Souza, G.F., Hassler, C.S., Ellwood, M.J., Vance, D.,
1154 2020. Cycling of zinc and its isotopes across multiple zones of the Southern
1155 Ocean: Insights from the Antarctic Circumnavigation Expedition. Geochim.
1156 Cosmochim. Acta 268, 310–324. https://doi.org/10.1016/j.gca.2019.09.039

1157 Sommer, S., Gier, J., Treude, T., Lomnitz, U., Dengler, M., Cardich, J., Dale, A.W.,
1158 2016. Depletion of oxygen, nitrate and nitrite in the Peruvian oxygen minimum
1159 zone cause an imbalance of benthic nitrogen fluxes. Deep. Res. Part I
1160 Oceanogr. Res. Pap. 112, 113–122. https://doi.org/10.1016/j.dsr.2016.03.001

1161 Stramma, L., Schmidtko, S., Levin, L.A., Johnson, G.C., 2010. Ocean oxygen minima
1162 expansions and their biological impacts. Deep. Res. Part I Oceanogr. Res. Pap.
1163 57, 587–595. https://doi.org/10.1016/j.dsr.2010.01.005

1164 Suess, E., Kulm, L.D., Killingley, J.S., 1987. Coastal upwelling and a history of
1165 organic-rich mudstone deposition off Peru. Geol. Soc. London, Spec. Publ. 26,
1166 181–197. https://doi.org/10.1144/GSL.SP.1987.026.01.11

1167 Suits, N.S., Arthur, M.A., 2000. Sulfur diagenesis and partitioning in Holocene Peru
1168 shelf and upper slope sediments. Chem. Geol. 163, 219–234.
1169 https://doi.org/10.1016/S0009-2541(99)00114-X

1170 Sundby, B., Anderson, L.G., Hall, P.O.J., Iverfeldt, Å., van der Loeff, M.M.R.,
1171 Westerlund, S.F.G., 1986. The effect of oxygen on release and uptake of cobalt,
1172 manganese, iron and phosphate at the sediment-water interface. Geochim.
1173 Cosmochim. Acta 50, 1281–1288. https://doi.org/10.1016/0016-7037(86)90411-
1174 4

1175 Sweere, T., van den Boorn, S., Dickson, A.J., Reichart, G.-J., 2016. Definition of new
1176 trace-metal proxies for the controls on organic matter enrichment in marine
1177 sediments based on Mn, Co, Mo and Cd concentrations. Chem. Geol. 441, 235–
1178 245. https://doi.org/10.1016/j.chemgeo.2016.08.028

1179 Tagliabue, A., Hawco, N.J., Bundy, R.M., Landing, W.M., Milne, A., Morton, P.L.,
1180 Saito, M.A., 2018. The Role of External Inputs and Internal Cycling in Shaping
1181 the Global Ocean Cobalt Distribution: Insights From the First Cobalt
1182 Biogeochemical Model. Global Biogeochem. Cycles 32, 594–616.
1183 https://doi.org/10.1002/2017GB005830

1184 Tankéré, S.P.., Muller, F.L.., Burton, J.., Statham, P.., Guieu, C., Martin, J.-M., 2001.
1185 Trace metal distributions in shelf waters of the northwestern Black Sea. Cont.
1186 Shelf Res. 21, 1501–1532. https://doi.org/10.1016/S0278-4343(01)00013-9

1187 Taylor, S.R., McLennan, S.M., 1995. The geochemical evolution of the continental
1188 crust. Rev. Geophys. 33, 241. https://doi.org/10.1029/95RG00262

1189 Tebo, B.M., 1991. Manganese(II) oxidation in the suboxic zone of the Black Sea.
1190 Deep Sea Res. Part A. Oceanogr. Res. Pap. 38, S883–S905.
1191 https://doi.org/10.1016/S0198-0149(10)80015-9

1192 Thamdrup, B., Glud, R.N., Hansen, J.W., 1994. Manganese oxidation and in situ
1193 manganese fluxes from a coastal sediment. Geochim. Cosmochim. Acta 58,
1194 2563–2570. https://doi.org/10.1016/0016-7037(94)90032-9

1195 Thamdrup, B., Dalsgaard, T., Revsbech, N.P., 2012. Widespread functional anoxia in
1196 the oxygen minimum zone of the Eastern South Pacific. Deep Sea Res. Part I
1197 Oceanogr. Res. Pap. 65, 36–45. https://doi.org/10.1016/j.dsr.2012.03.001

1198 Theberge, M., Luther, G.W., Farrenkopf, A.M., 1997. On the existence of free and
1199 metal complexed sulfide in the Arabian Sea and its oxygen minimum zone 44,
1200 1381–1390. https://doi.org/10.1016/S0967-0645(97)00012-X

1201 Tribovillard, N., Algeo, T.J., Lyons, T., Riboulleau, A., 2006. Trace metals as
1202 paleoredox and paleoproductivity proxies: An update. Chem. Geol. 232, 12–32.
1203 https://doi.org/10.1016/j.chemgeo.2006.02.012

1204 Turetta, C., Capodaglio, G., Cairns, W., Rabar, S., Cescon, P., 2005. Benthic fluxes
1205 of trace metals in the lagoon of Venice. Microchem. J. 79, 149–158.
1206 https://doi.org/10.1016/j.microc.2004.06.003

1207 Twining, B.S., Baines, S.B., Bozard, J.B., Vogt, S., Walker, E.A., Nelson, D.M., 2011.
1208 Metal quotas of plankton in the equatorial Pacific Ocean. Deep Sea Res. Part II
1209 Top. Stud. Oceanogr. 58, 325–341. https://doi.org/10.1016/j.dsr2.2010.08.018

1210 Ulloa, O., Escribano, R., Hormazabal, S., Quiñones, R.A., González, R.R., Ramos,
1211 M., 2001. Evolution and biological effects of the 1997-98 El Niño in the upwelling
1212 ecosystem off northern Chile. Geophys. Res. Lett. 28, 1591–1594.
1213 https://doi.org/10.1029/2000GL011548

1214 van de Velde, S.J., Hylén, A., Kononets, M., Marzocchi, U., Leermakers, M.,
1215 Choumiline, K., Hall, P.O.J., Meysman, F.J.R., 2020. Elevated sedimentary
1216 removal of Fe, Mn, and trace elements following a transient oxygenation event in
1217 the Eastern Gotland Basin, central Baltic Sea. Geochim. Cosmochim. Acta 271,
1218 16–32. https://doi.org/10.1016/j.gca.2019.11.034

1219 Vance, D., Archer, C., Bermin, J., Perkins, J., Statham, P.J., Lohan, M.C., Ellwood,
1220 M.J., Mills, R.A., 2008. The copper isotope geochemistry of rivers and the
1221 oceans. Earth Planet. Sci. Lett. 274, 204–213.
1222 https://doi.org/10.1016/j.epsl.2008.07.026

1223 Vance, D., Little, S.H., Archer, C., Cameron, V., Andersen, M.B., Rijkenberg, M.J.A.,
1224 Lyons, T.W., 2016. The oceanic budgets of nickel and zinc isotopes: the
1225 importance of sulfidic environments as illustrated by the Black Sea. Philos.
1226 Trans. R. Soc. A Math. Phys. Eng. Sci. 374, 20150294.
1227 https://doi.org/10.1098/rsta.2015.0294

1228 Vedamati, J., Chan, C., Moffett, J.W., 2014. Distribution of dissolved manganese in

the Peruvian Upwelling and Oxygen Minimum Zone. Geochim. Cosmochim. Acta 156, 222–240. https://doi.org/10.1016/j.gca.2014.10.026

Vijayaraghavan, K., Jegan, J., Palanivelu, K., Velan, M., 2005. Biosorption of copper, cobalt and nickel by marine green alga Ulva reticulata in a packed column. Chemosphere 60, 419–426. https://doi.org/10.1016/j.chemosphere.2004.12.016

Westerlund, S.F.G., Anderson, L.G., Hall, P.O.J., Iverfeldt, Å., Van Der Loeff, M.M.R., Sundby, B., 1986. Benthic fluxes of cadmium, copper, nickel, zinc and lead in the coastal environment. Geochim. Cosmochim. Acta 50, 1289–1296. https://doi.org/10.1016/0016-7037(86)90412-6

Xie, R.C., Rehkämper, M., Grasse, P., van de Flierdt, T., Frank, M., Xue, Z., 2019. Isotopic evidence for complex biogeochemical cycling of Cd in the eastern tropical South Pacific. Earth Planet. Sci. Lett. 512, 134–146. https://doi.org/10.1016/j.epsl.2019.02.001

Zimmerman, A.J., Weindorf, D.C., 2010. Heavy Metal and Trace Metal Analysis in Soil by Sequential Extraction: A Review of Procedures. Int. J. Anal. Chem. 2010, 1–7. https://doi.org/10.1155/2010/387803

Tables and figures

Table 1: Sedimentary trace metal excess accumulation ($TM_{xs}MAR$) and the contribution of trace metal delivery to the sediment by diffusion and via incorporation by phytoplankton and deposition of organic particles (see section 2.4 for a detailed description how these fluxes were calculated).

Station	Diffusive flux (µmol m^{-2} y^{-1})						Input via phytoplankton [1] (µmol m^{-2} y^{-1})						Excess accumulation [2] (µmol m^{-2} y^{-1})					
	Mn	Co	Ni	Cu	Zn	Cd	Mn	Co	Ni	Cu	Zn	Cd	Mn	Co	Ni	Cu	Zn	Cd
1	-551	-2.57	-43.2	-2.82	1993	-1.84	112/ 656	7.55/ 44.4	39.8/ 234	15.1/ 88.8	32.3/ 190	8.34/ 49.0	-1160	-123	145	594	2170	261
3	-244	-1.66	-17.6	10.6	688	0.83	65.1/ 233	4.41/ 15.8	23.2/ 83.0	8.82/ 31.5	18.9/ 67.3	4.87/ 17.4	-511	-27.0	158	144	415	110
4	-390	-4.05	7.63	-0.40	-20.3	0.54	20.8/ 86.6	1.41/ 5.86	7.41/ 30.9	2.81/ 11.7	6.02/ 25.1	1.56/ 6.48	-386	-18.3	117	61.5	212	63.0
5	-160	-2.33	-11.5	-1.94	733	0.63	76.3/ 103	5.17/ 7.00	27.2/ 36.8	10.3/ 14.0	22.1/ 29.8	5.71/ 7.71	-279	-11.0	180	91.8	165	63.0
6	-128	-3.96	-71.3	12.7	20.9	0.55	48.1/ 87.4	3.26/ 5.92	17.2/ 31.2	6.51/ 11.8	13.9/ 25.3	3.60/ 6.54	-100	-3.44	87.0	32.5	57.8	23.6
9	-26.4	-0.13	-35.7	-3.47	117	0.30	19.7/ 42.9	1.34/ 2.90	7.04/ 15.3	2.67/ 5.81	5.71/ 12.4	1.48/ 3.21	-880	-33.3	249	168	356	5.78

[1] Determined by multiplying the TM:C ratio in average phytoplankton (Moore et al., 2013) with particulate organic carbon rain rates (maximum values) and organic carbon accumulation rates (minimum values) for each site (data from Dale et al. (2015b)).

[2] Excess accumulation was calculated from Eq. 2 by multiplying the trace metal excess (calculated after Brumsack (2006) (Eq. 1)) with the sediment mass accumulation rate for each site (Dale et al., 2020).

Figure captions:

Figure 1: Sampling locations (stars) and station numbers on the Peruvian continental margin during cruises M136 and M137. Water depths and station coordinates are summarised in Tab. S.1.

Figure 2: Dissolved oxygen (O_2), nitrate (NO_3^-) and nitrite (NO_2^-) concentrations in the water column on the Peruvian shelf and slope during the time of sampling (from Plass et al. (2020)).

Figure 3: Pore water dissolved trace metal concentrations. The arrow represents the bottom water concentration. Data for cadmium (Cd) and hydrogen sulphide (H_2S) are from Plass et al. (2020).

Figure 4: Total trace metal contents in sediments determined from total digestions (red dashed line) and trace metal contents in different fractions determined from sequential extractions (HCl, HNO_3, HF).

Figure 5: Enrichment of trace metals (TM_{xs}) compared to the lithogenic background against water depth. The average particulate organic carbon content is also plotted. Numbers in the upper panel depict station numbers.

Fig. 6: Cross plots of trace metal contents in the combined HCl-fractions (TMs associated with monosulphides, (oxyhydr)oxides, carbonates and hydrous aluminosilicates) and HNO_3-fraction (TMs associated with pyrite and organic matter) from sequential extractions versus total sulphur (TS) and particulate organic carbon (POC) contents. Since no Cd was present in the HNO_3-fraction it is not shown.

Figure 7: Sedimentary trace metal excess accumulation or loss ($TM_{xs}MAR$) (diamonds) and the contribution of trace metal delivery to or removal from the sediment via different pathways; diffusion across the sediment-water interface (blue) and trace metal incorporation by phytoplankton and delivery to the sediment with organic matter (green) (displayed is the maximum value, see Methods). Positive values represent fluxes into the sediment whereas negative values represent fluxes out of the sediment. Numbers in the upper panel depict station numbers.

Figure 8: Cobalt to manganese ratio (Co:Mn) in sediment pore waters, average phytoplankton (Moore et al., 2013) and andesitic crust (Taylor and McLennan, 1995).

Figure 9: Nickel to particulate organic carbon ratio (Ni:POC) within bulk sediments and average phytoplankton (Moore et al., 2013).

Figure 10: Schematic sketch illustrating the main pathways and processes by which TMs are lost from or delivered to Peru margin sediments. Straight arrows represent solid phase transport, curved arrows represent dissolved transport. Dashed arrows denote possible transport and precipitation processes that are uncertain but can be potentially important. The arrow size depicts the relative magnitude of the flux. The lower pannel illustrates net-depletion (upward directed arrow) or net-enrichment (downward directed arrow) of the different trace metals in the sediment.

Figure 1

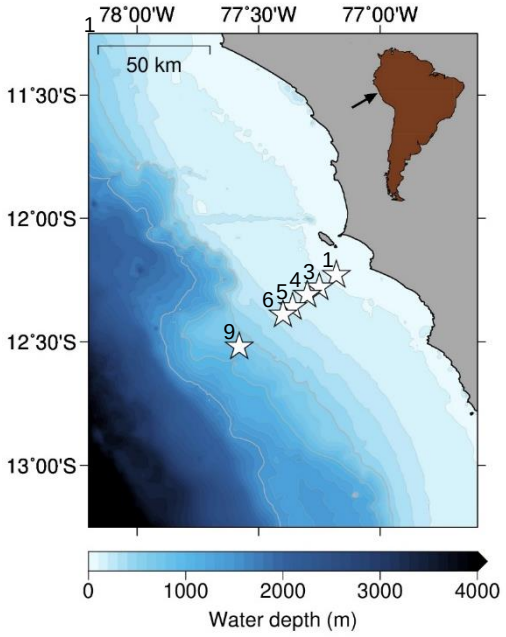

Figure 2

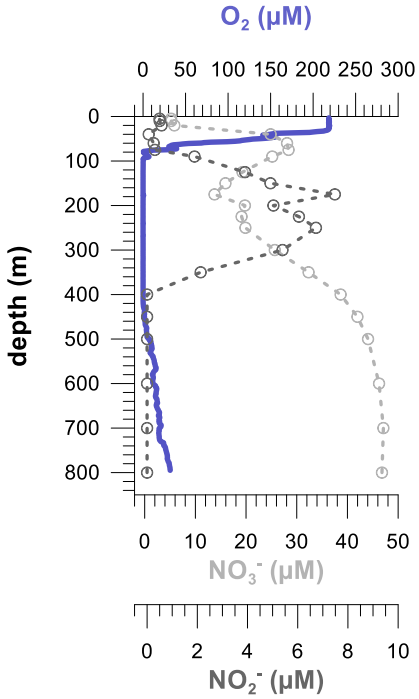

Figure 3

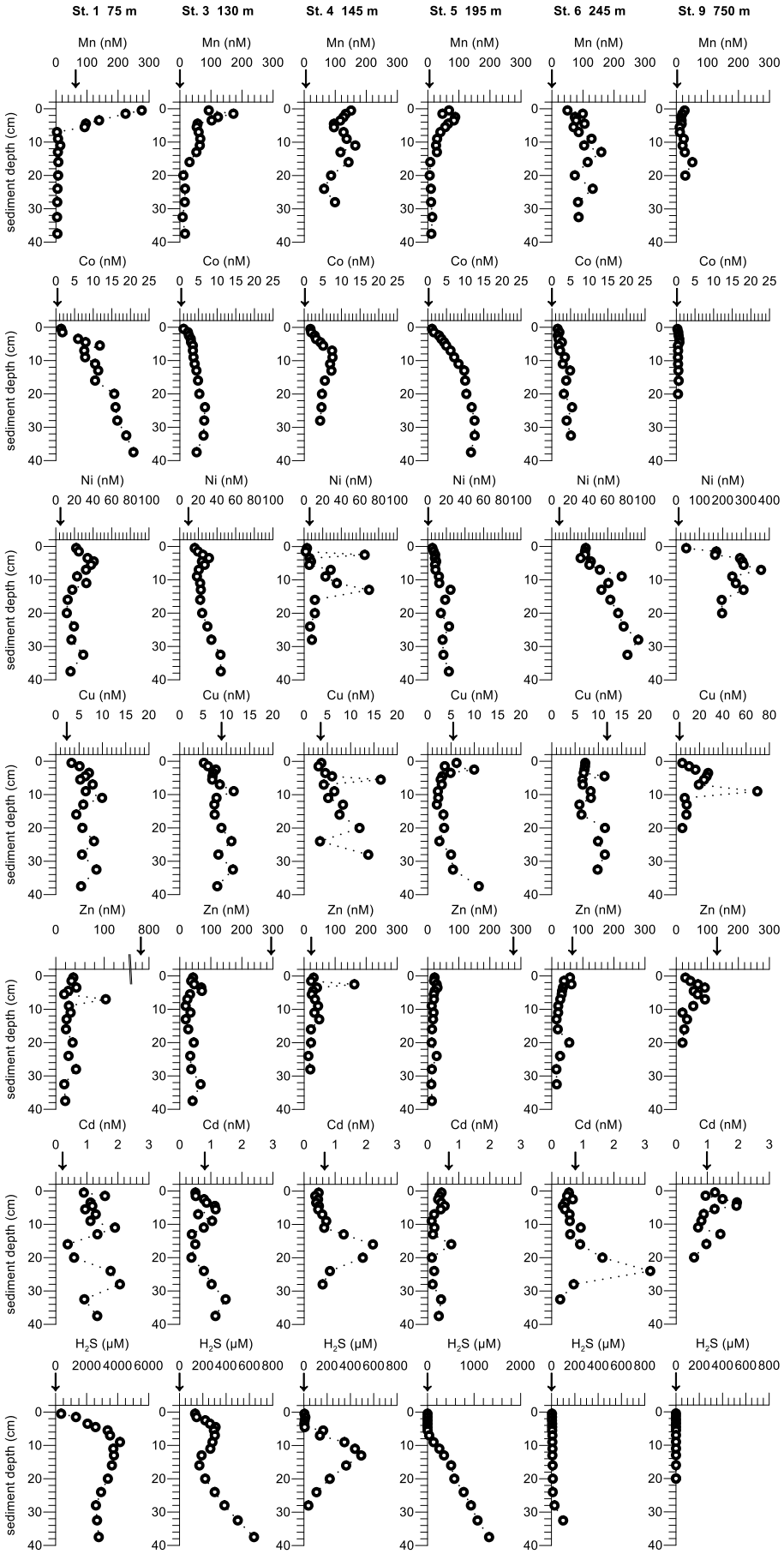
St. 1 75 m
St. 3 130 m
St. 4 145 m
St. 5 195 m
St. 6 245 m
St. 9 750 m
Mn (nM)
Co (nM)
Ni (nM)
Cu (nM)
Zn (nM)
Cd (nM)
H2S (µM)
sediment depth (cm)

Figure 4

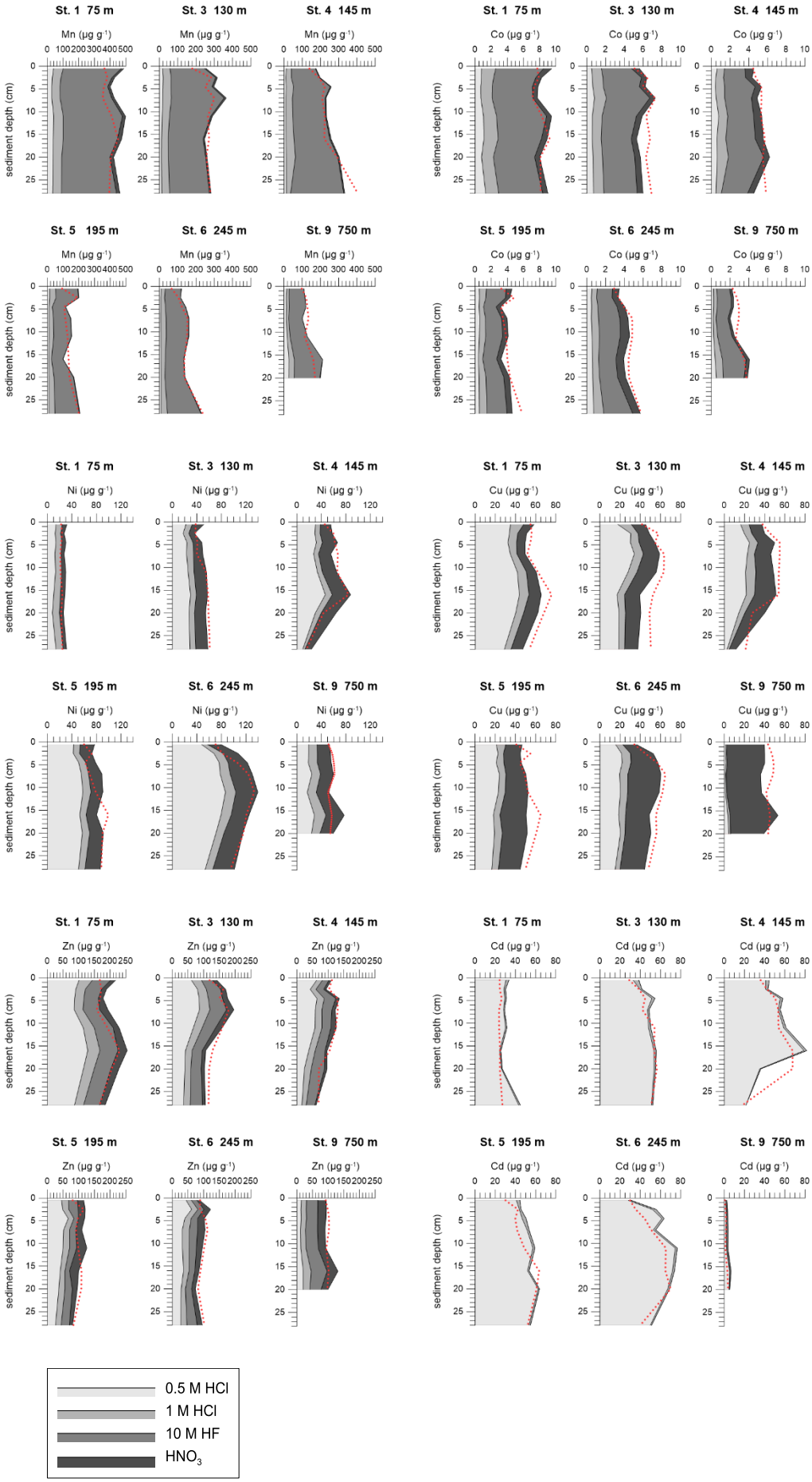
St. 1 75 m
St. 3 130 m
St. 4 145 m
St. 5 195 m
St. 6 245 m
St. 9 750 m
Mn (µg g-1)
Co (µg g-1)
Ni (µg g-1)
Cu (µg g-1)
Zn (µg g-1)
Cd (µg g-1)
sediment depth (cm)
0.5 M HCl
1 M HCl
10 M HF
HNO3

Figure 5

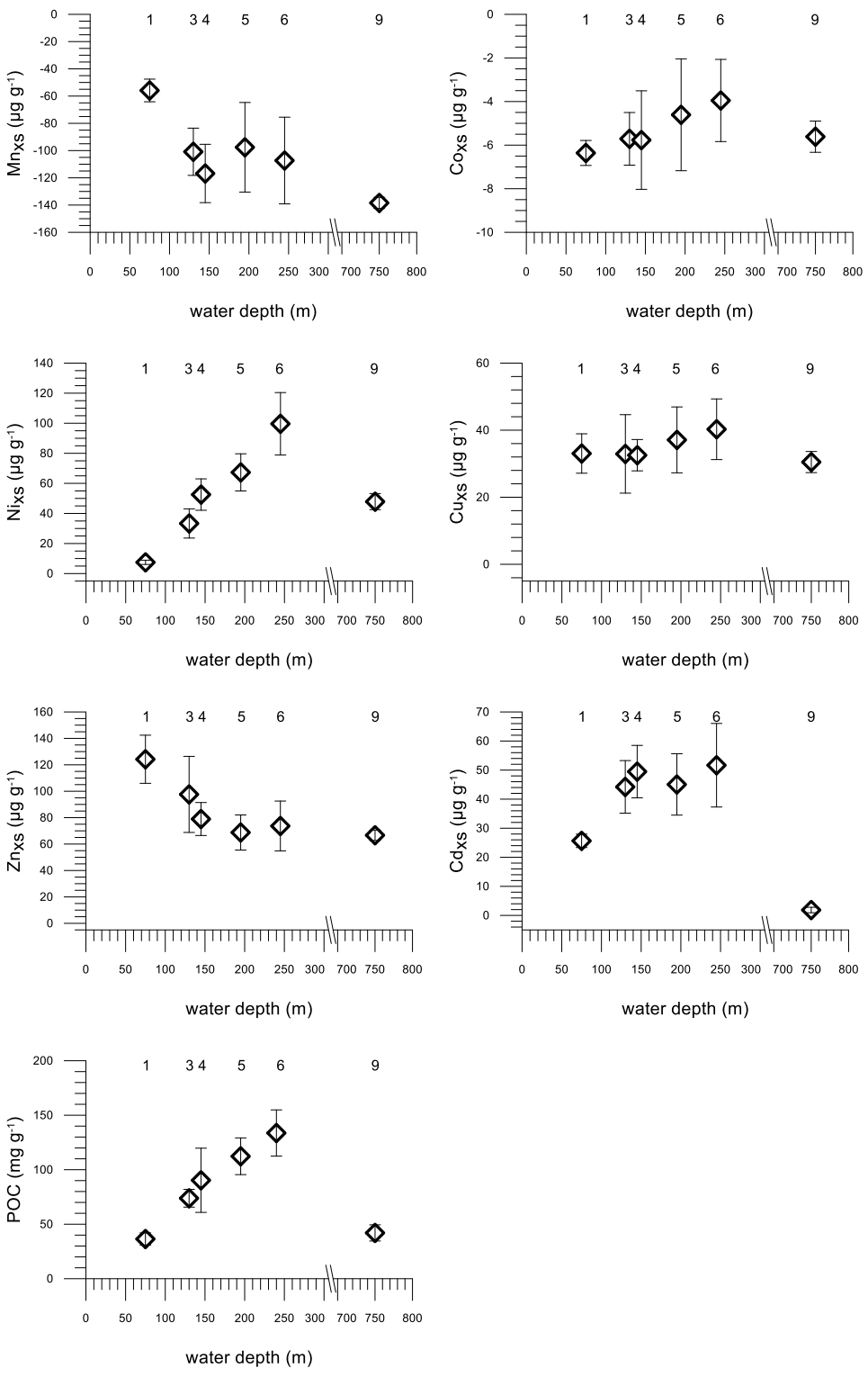
1
3 4
5
6
9
Mn_{xs} (µg g^{-1})
Co_{xs} (µg g^{-1})
Ni_{xs} (µg g^{-1})
Cu_{xs} (µg g^{-1})
Zn_{xs} (µg g^{-1})
Cd_{xs} (µg g^{-1})
POC (mg g^{-1})
water depth (m)

Figure 6

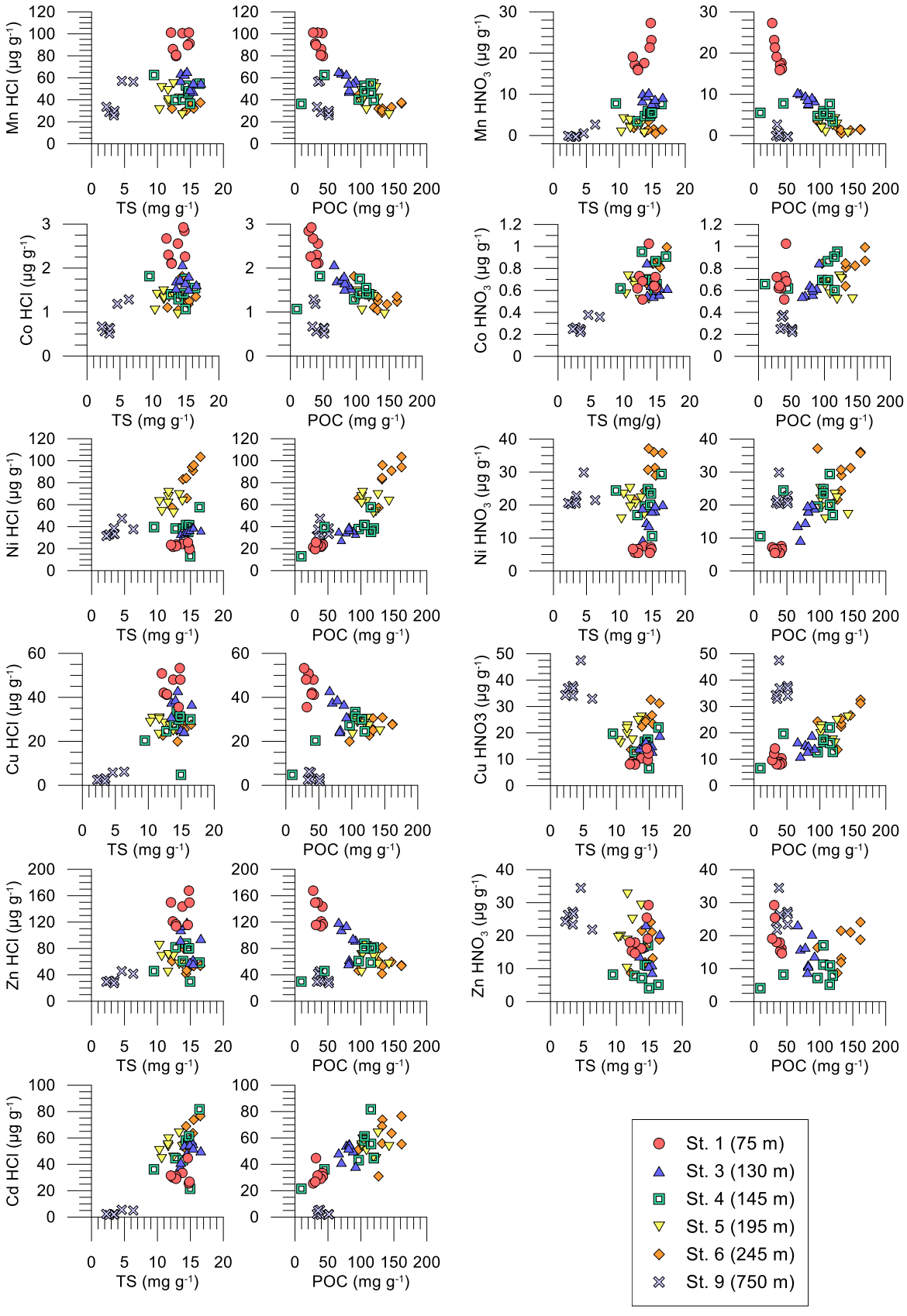
Mn HCl (µg g-1)
Mn HNO3 (µg g-1)
Co HCl (µg g-1)
Co HNO3 (µg g-1)
Ni HCl (µg g-1)
Ni HNO3 (µg g-1)
Cu HCl (µg g-1)
Cu HNO3 (µg g-1)
Zn HCl (µg g-1)
Zn HNO3 (µg g-1)
Cd HCl (µg g-1)
TS (mg g-1)
TS (mg/g)
POC (mg g-1)
St. 1 (75 m)
St. 3 (130 m)
St. 4 (145 m)
St. 5 (195 m)
St. 6 (245 m)
St. 9 (750 m)

Figure 7

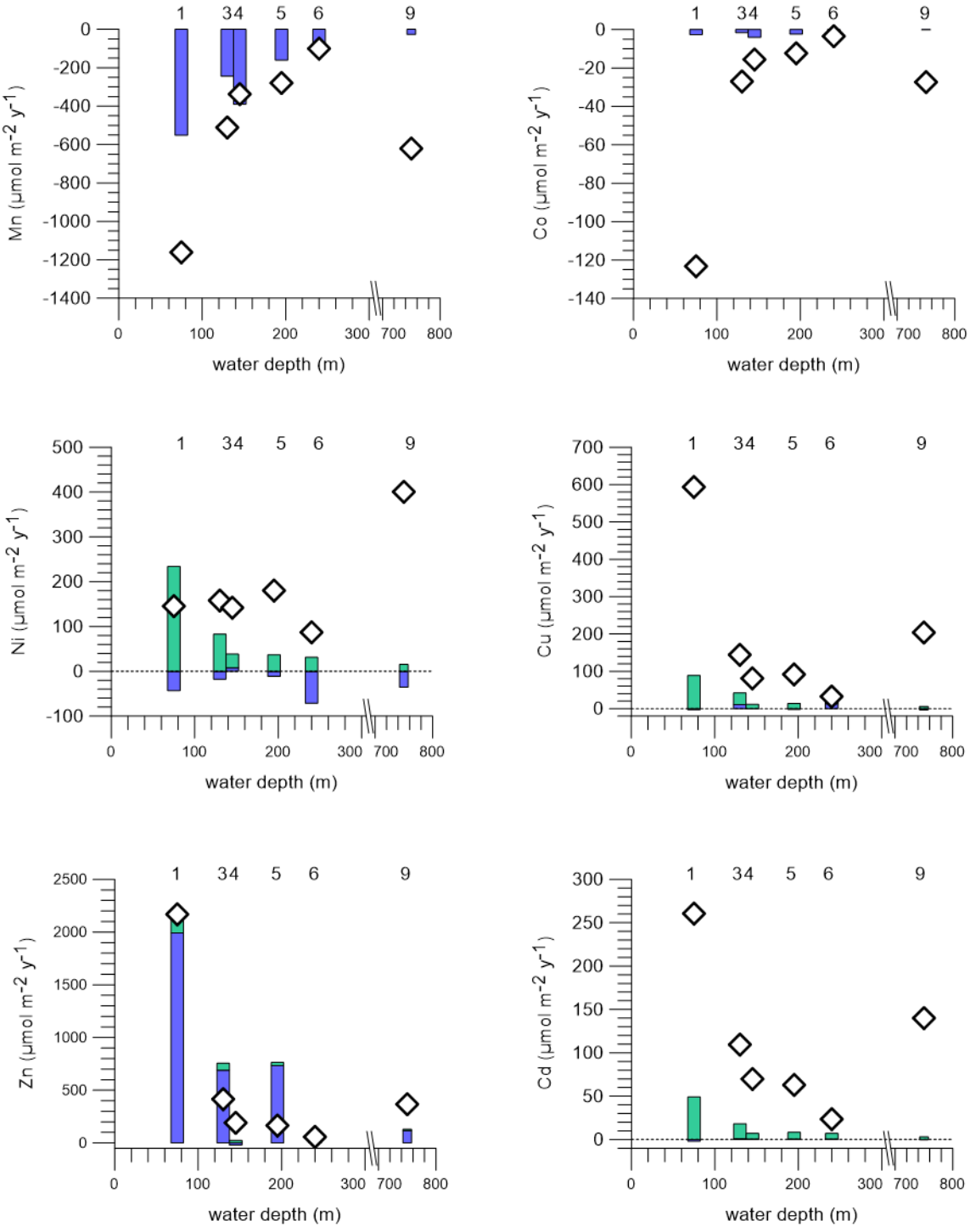
1
34
5
6
9
Mn (µmol m-2 y-1)
Co (µmol m-2 y-1)
Ni (µmol m-2 y-1)
Cu (µmol m-2 y-1)
Zn (µmol m-2 y-1)
Cd (µmol m-2 y-1)
water depth (m)
0
100
200
300
700
800
TMxsMAR
diffusive flux
input via phytoplankton

Figure 8

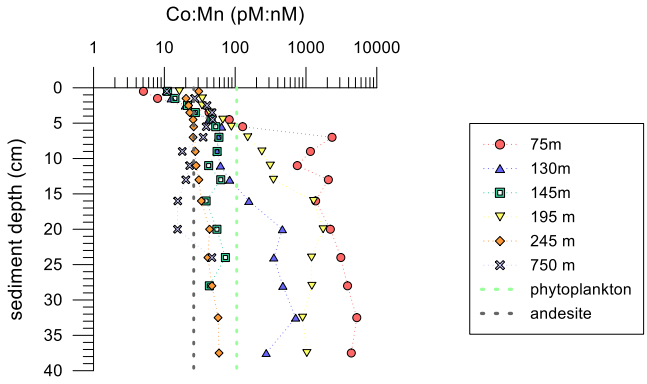

Figure 9

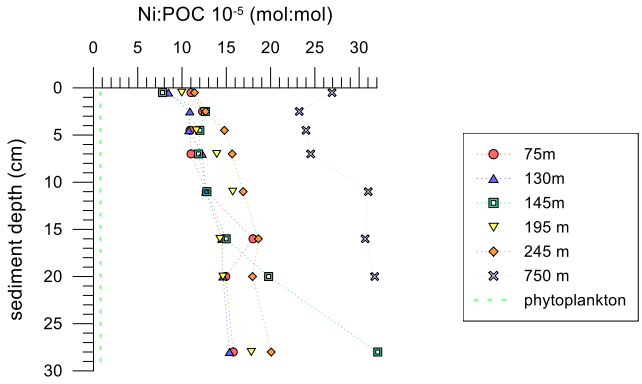

Figure 10

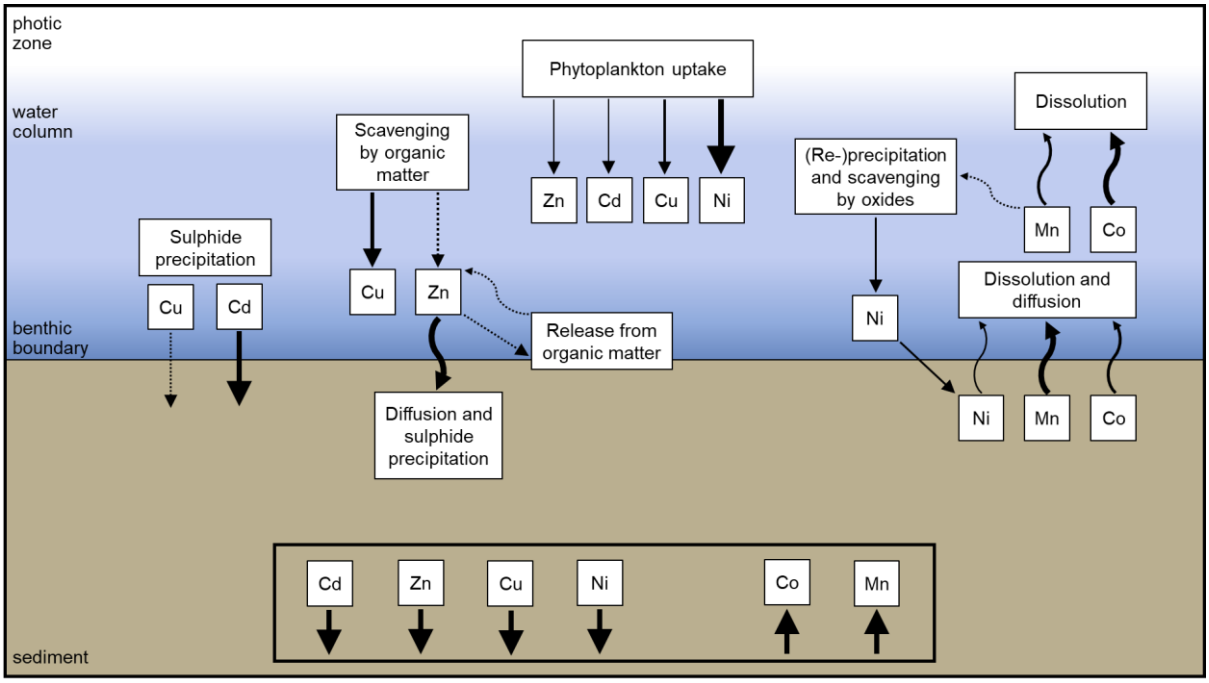
photic zone
water column
benthic boundary
sediment
Phytoplankton uptake
Zn
Cd
Cu
Ni
Scavenging by organic matter
Cu
Zn
Release from organic matter
Diffusion and sulphide precipitation
Sulphide precipitation
Cu
Cd
(Re-)precipitation and scavenging by oxides
Ni
Dissolution
Mn
Co
Dissolution and diffusion
Ni
Mn
Co
Cd
Zn
Cu
Ni
Co
Mn

Supplement

Table S.1: Station coordinates and water depth.

Station	Water depth (m)	Latitude	Longitude
1	75	12°13.519' S	77°10.793' W
3	130	12°16.678' S	77°14.954' W
4	145	12°18.709' S	77°17.796' W
5	195	12°21.504' S	77°21.699' W
6	245	12°23.301' S	77°24.182' W
9	750	12°34.896' S	77°35.013' W

Table S.2: Accuracy of replicate ICP-MS measurements (n = 7) of certified reference seawater standards NASS-7 and CASS-6.

	NASS-7 certified value	NASS-7 measured value	CASS-6 certified value	CASS-6 measured value
Mn (µg l^{-1})	0.75 ± 0.06	0.83 ± 0.11	2.22 ± 0.12	2.22 ± 0.40
Co (µg l^{-1})	0.146 ± 0.0014	0.146 ± 0.0054	0.0627 ± 0.0052	0.0630 ± 0.0105
Ni (µg l^{-1})	0.248 ± 0.018	0.247 ± 0.039	0.418 ± 0.040	0.438 ±0.050
Cu (µg l^{-1})	0.199 ± 0.014	0.216 ± 0.012	0.530 ± 0.032	0.521 ± 0.051
Zn (µg l^{-1})	0.42 ± 0.08	0.43 ± 0.08	1.27 ± 0.018	1.29 ± 0.092
Cd (µg l^{-1})	0.0161 ± 0.0016	0.0162 ± 0,0024	0.0217 ± 0.0018	0.0216 ± 0.0016

Table S.3: Trace metal contents of in-house reference standard (OMZ 2) from total digestions and the total trace metal content from sequential extractions (n = 3). Reference values of trace metal contents in the certified standard MESS-3 and trace metal contents from total digestions and the sum content of the sequential extractions (n = 17).

	Mn ($\mu g\ g^{-1}$)	**Co ($\mu g\ g^{-1}$)**	**Ni ($\mu g\ g^{-1}$)**	**Cu ($\mu g\ g^{-1}$)**	**Zn ($\mu g\ g^{-1}$)**	**Cd ($\mu g\ g^{-1}$)**	**Al ($\mu g\ g^{-1}$)**
OMZ 2 Reference value (total digestion)	253.3 ± 2.8	6.3 ± 0.1	49.8 ± 1.0	35.3 ± 0.5	98.3 ± 8.8	26.5 ± 0.3	-
OMZ 2 sequential extractions	251.6 ± 3.3	5.7 ± 0.0	47.2 ± 2.7	28.0 ± 0.5	82.3 ± 3.1	27.2 ± 0.5	-
MESS-3 Reference value	324 ± 12	14.4 ± 2.0	46.9 ± 2.2	33.9 ± 1.6	159 ± 8	0.24 ± 0.01	8.59 ± 0.23
MESS-3 total digestion	323 ± 5	14.2 ± 0.3	46.45 ± 0.1	33.1 ± 1.5	156 ± 5	0.24 ± 0.01	8.59 ± 0.11
MESS-3 sequential extractions	311 ± 1	12.2 ± 0.3	20.7 ± 3.5	28.3 ± 8.4	148 ± 2	0.96 ± 0.38	-

Table S.4: Average trace metal and particulate organic carbon content in sediments of all samples over each core.

Station	Water depth (m)	Trace metal content (µg g^{-1})							Particulate organic carbon content (mg g^{-1})	Total sulphur content (mg g^{-1})
		Mn	Co	Ni	Cu	Zn	Cd	Al		
1	75	386	7.89	23.3	57.6	176	25.8	54533	36.4	13.3
3	130	275	6.50	46.8	53.8	142	44.4	46424	73.8	14.8
4	145	234	4.93	56.2	44.7	130	44.8	44605	90.4	14.1
5	195	161	4.27	76.6	51.5	99.1	45.2	31966	112	12.0
6	245	156	4.61	109	54.9	105	51.8	32555	134	14.7
9	750	130	3.12	57.5	45.4	98.2	1.96	33190	42.1	3.81

Table S.5a: Input data for diffusive flux calculations (Eq. (3) in main text).

Station	Water depth (m)	Bottom water concentration (nM)						Concentration at sediment surface (nM)					
		Mn	Co	Ni	Cu	Zn	Cd	Mn	Co	Ni	Cu	Zn	Cd
1	75	63.7	0.42	4.96	2.35	775	0.22	276	1.40	21.9	3.37	36.1	0.90
3	130	0.16	0.37	9.92	8.97	294	0.81	93.0	0.99	16.1	5.17	42.7	0.65
4	145	5.60	0.19	5.97	3.57	23.2	0.66	151	1.67	3.09	3.71	30.6	0.47
5	195	5.43	0.22	0.50	5.47	276	0.68	68.0	1.11	5.02	6.18	22.0	0.44
6	245	0	0	8.04	11.9	66.3	0.76	50.1	1.53	36.4	7.18	58.4	0.55
9	750	2.74	0.17	10.8	2.29	131	0.99	26.6	0.29	43.4	5.23	29.5	1.25

Table S.5b: Molecular diffusion coefficients in seawater (Li and Gregory, 1974), adjusted to in-situ temperature, pressure and salinity, used for diffusive flux calculations (Eq. (3) in main text).

Station	Molecular diffusion coefficients 10^{-6} (cm^2 s^{-1})					
	Mn	Co	Ni	Cu	Zn	Cd
1	4.42	4.49	4.36	4.71	4.59	4.60
3	4.38	4.45	4.33	4.67	4.56	4.57
4	4.42	4.49	4.36	4.71	4.50	4.61
5	4.26	4.33	4.20	4.54	4.79	4.44
6	4.24	4.31	4.19	4.52	4.41	4.42
9	2.36	2.40	2.33	2.52	2.46	2.46

Table S.5c: Porosity used for diffusive flux calculations (Eq. (3) in main text) and in-situ temperature, pressure and salinity data used to adjust molecular diffusion coefficients (Table S.5b).

Station	Water depth	Porosity	Temperature (°C)	Pressure (bar)	Salinity
1	75	0.93	16.2	8.77	35.1
3	130	0.95	14.0	13.9	35.0
4	145	0.96	14.0	15.4	35.0
5	195	0.96	13.2	20.4	34.9
6	245	0.95	13.3	25.6	34.9
9	750	0.74	6.28	75.0	34.6